Dissolved Organic Matter from a colloidal perspective

Andersson, Erika

2023

Document Version:
Publisher's PDF, also known as Version of record

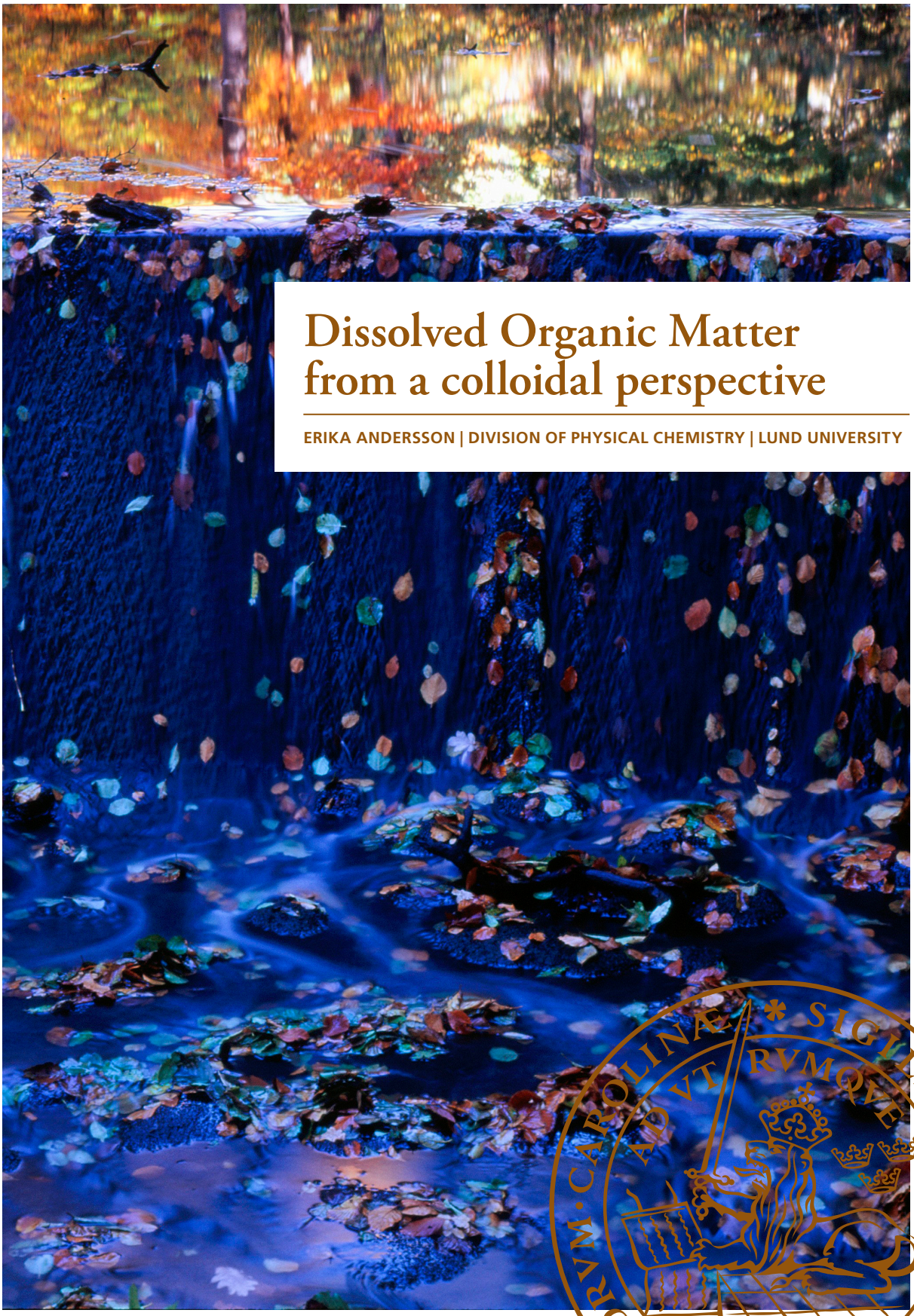

Dissolved Organic Matter from a colloidal perspective

ERIKA ANDERSSON | DIVISION OF PHYSICAL CHEMISTRY | LUND UNIVERSITY

Dissolved Organic Matter from a colloidal perspective

Dissolved Organic Matter from a colloidal perspective

by Erika Andersson

LUND
UNIVERSITY

DOCTORAL DISSERTATION

by due permission of the Faculty of Science, Lund University, Sweden.
To be defended on Friday, the 9th of June 2023 at 09:15 in Lecture hall A at the Department of Chemistry, Lund University.

Faculty opponent

Prof. Walter Richtering
IPC, RWTH Aachen University, Germany

Organization
LUND UNIVERSITY

Department of Chemistry
Box 124
SE–221 00 LUND
Sweden

Author(s)
Erika Andersson

Document name
DOCTORAL DISSERTATION

Date of disputation
2023-06-09

Sponsoring organization
Swedish Research Council
Grant number: 2018-05513

Title and subtitle
Dissolved Organic Matter from a colloidal perspective

Abstract
Dissolved organic matter (DOM) is considered the most bioavailable fraction of soil, and thus play a key role in the cycling of carbon. Because of its mobility, DOM also forms the connection between terrestrial and aquatic systems, and constitutes an important vector for nutrients and contaminants. DOM is in this thesis operationally defined as the organic matter in an aqueous solution which is not retained upon filtration using a pore size of 0.2µm. This means that DOM is a heterogeneous mixture of different chemical components, ranging in size from small molecules up to colloidal particles of a few hundred nanometres.
In this thesis, we have characterised DOM from the molecular to colloidal length scale, using a combination of spectroscopy, microscopy and scattering techniques. The DOM was obtained by extraction of soil from the organic layer of a boreal spruce forest. We found that the dominant chemical component of DOM was carbohydrates, and that about half of the organic carbon was present in colloidal form. The structure of the DOM colloids depended on the extraction procedure used. Large dense aggregates observed at room temperature and below could be dispersed into smaller components by increasing the temperature or pH. Additionally, we studied the bacterial decomposition of DOM and found that the colloidal fraction remained intact, while small molecules were readily decomposed. We have also assessed interactions between DOM and hematite nanoparticles, using neutron scattering. Here, we found that the low molecular weight fraction of DOM induces charge reversal and aggregation of the hematite particles. Our combined results show that the colloidal fraction of DOM needs to be considered when assessing DOM bioavailability and mobility.

Key words
Dissolved Organic Matter, colloids, microbial decomposition, hematite nanoparticles, soil, small angle scattering, light scattering, ^{1}H NMR

Classification system and/or index terms (if any)

Supplementary bibliographical information

Language
English

ISSN and key title

ISBN
978-91-7422-956-1 (print)
978-91-7422-957-8 (pdf)

Recipient's notes

Number of pages
221

Price

Security classification

Signature _____ Date 2023-04-20

Dissolved Organic Matter from a colloidal perspective

by Erika Andersson

LUND
UNIVERSITY

This doctoral thesis is constructed as a summary of research papers and consists of two parts. An introductory text puts the research work into context and summarises the main conclusions of the papers. Then, the research publications themselves are reproduced. The research papers may either have been already published or are manuscripts at various stages.

Front cover: Photo from Pålsjö damm by Martin Aurell
Back cover: Photo of SAXS capillaries with DOM and mineral samples

Faculty of Science, Department of Chemistry, Division of Physical Chemistry

ISBN: 978-91-7422-956-1 (print)
ISBN: 978-91-7422-957-8 (pdf)

Printed in Sweden by Media-Tryck, Lund University, Lund 2023

Media-Tryck is a Nordic Swan Ecolabel certified provider of printed material. Read more about our environmental work at www.mediatryck.lu.se

MADE IN SWEDEN

"Where my understanding is limited nature takes over"
– Carmen Chor Faunbäck

Table of Contents

Acknowledgements

This journey would not have been possible without the help and support of my supervisors. Thank you **Ulf** for convincing me to hop on, constantly providing new challenges, and for taking good care of your students and group members. And thanks to **Per** and **Anders**, for offering new perspectives, valuable feedback and help with things beyond the understanding of a physical chemist.

I also want to thank all my co-authors and collaborators for the great work we have accomplished. **Viktoriia**, thanks for everything you taught me and the long discussions about life in general, it was a long journey but we both made it out! **Luigi**, you started all of this and then you left... Thanks for getting us to talk to the biologists, sharing your knowledge and making sure I finally got to Italy. Thanks also to **Marloes** and **Lars** for welcoming me to Uppsala and providing yet another perspective on DOM, **Henrik**, **Abhishek**, **Ralf** and **Olga** for the good collaboration.

Dimitri, **Michiel**, **Edith** and **Lettice**, thank you for all the interesting discussions, insights on soil ecology, helping me find things and figure out how equipment works.

A big thank you to the fkem permanent staff for taking so many burdens of our PhD shoulders. **Maria S**, **Maria L** (and previously Helena), **Chris** and **Peter**, you deserve a lot of appreciation for your work, which makes it possible for us to do ours. The same goes for **Anna** at microbial ecology, creating order in the chaos, **Sofia** performing the elemental analysis (whenever the instrument found it appropriate to collaborate) and **Göran** for keeping the NMR working. Thank you also to **Karin** for helping me with the ALV, giving me the opportunity to develop my teaching and always being cheerful and supporting; as well as **Anna** for keeping track of our ISPs and giving me the opportunity of this journey in the first place.

A warm thank you to the Ulf-group for all the support, fun times and interesting Friday meetings. Thank you **Birte** for sharing all your scattering knowledge and making sure I kick-started my academic journey in the best possible way. **Axel**, thank you for always helping out, making sure I am writing this in LaTeX and being awesome. **Marija**, thank you for always being so kind and caring and up for a chat, and for still hanging around! **Veronica**, thank you for the laughs and smiles and beamtime survival. Thanks also to all the rest of you passing through for longer or shorter time during these years!

The work days would have been far to long without coffee (tea?) breaks and good company. Thank you **Jen** for your happy smiles, the nice chats and travel company, **Simon** for good teaching team work, **Tommy** for long discussions over the troubles of life, **Marco** for being a wonderful person, **Davide** for welcoming us to Bari, and

to all the rest of you at the **Physical Chemistry division**! Thanks also to the **PhDs at microbial ecology** for the fun activities and for welcoming me in the soil community.

I am truly grateful for all the support and encouragement I have received from my family and my friends during this journey. To come home, is always the best recovery. **Nanogänget**, thank you for making sure fun things are happening to get my mind of work, and for all the long discussions about life and what to do with it. Finally, **Martin**, you get to hear all the complaints and yet you are my biggest support. Thank you for always standing by my side.

Popular Science Summary

Think about a carbon atom. In the atmosphere it exists as carbon dioxide, and through photosynthesis it is taken up by a plant and becomes part of a leaf. Autumn comes and the leaf falls to the ground and turns into litter. The fate of that carbon atom will now depend on decomposition processes. It might turn back into carbon dioxide within a few months and return to the atmosphere, or it might stay in the soil for hundreds of years. Soil stores roughly twice as much carbon as all biomass and the atmosphere combined. We would like that carbon, and preferably even more, to stay there. Because as we have learnt in the recent decades, disturbing the balance of the carbon cycle will have devastating effects on our climate.

It is therefore important for us to understand the mechanisms that control the preservation of carbon in soil and other ecosystems. Such knowledge can help us improve carbon sequestration and predictions of the effects a changing climate might have. It is also important for questions concerning farming, soil erosion and the quality of drinking water. And yet, we cannot explain what controls the fate of that carbon atom.

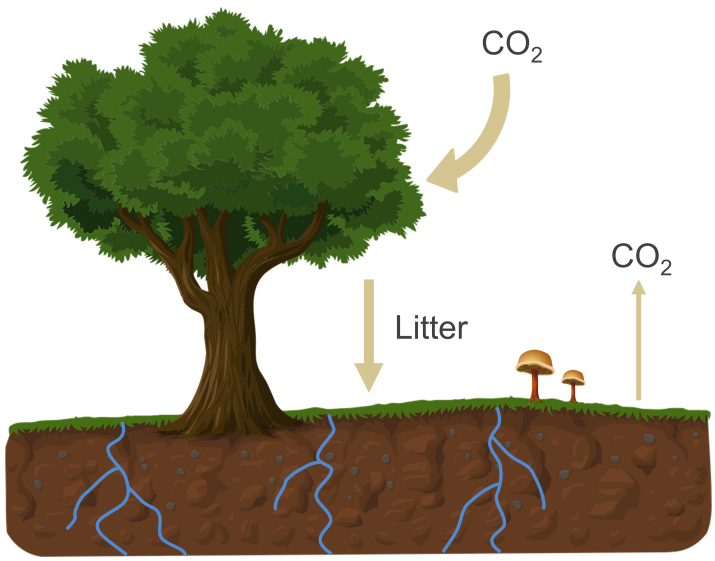

Schematic illustration of the carbon cycle.

The remains of living organisms are called organic matter. This is a material rich in carbon which microbes, such as bacteria and fungi, decompose to obtain energy and nutrients. The fraction of organic matter which should be the easiest for them to decompose is called dissolved organic matter (DOM) and is the topic of this thesis.

DOM is defined as the organic material in a water solution which can pass through a filter with a pore size of a few hundred nanometres. This means DOM is a mixture of many different chemical components ranging in size from individual small molecules up to suspended particles called colloids.

A lot of work has been put into understanding the chemistry of DOM, how it affects microbial decomposition and its role in the interactions between DOM and soil minerals. However, less is known about the physical structure of DOM, in particular of DOM colloids, and how structure might affect the fate of DOM. The work described in this thesis focused on characterising DOM, both chemically using spectroscopy techniques, and physically using scattering techniques. This combination allows access to information about DOM, from small molecules up to colloids. The conclusions drawn from this characterisation were then used to understand studies on bacterial decomposition of DOM, as well as the interactions taking place when DOM is mixed with mineral particles.

We have found that chemically, DOM is dominated by carbohydrates, meaning large sugar molecules which should be an important source of energy for microbes. Around half of the DOM carbon is present as colloids, and the size and physical structure of the colloids change depending on physical and chemical conditions. At ambient temperature, compact clusters are observed. When the temperature or pH is increased, these clusters disperse into smaller components. Feeding the DOM to bacteria, about half of the carbon was decomposed, but the colloids remained intact. When mixing the DOM with mineral particles, the colloids were observed to be unaffected, while the small molecules seemed to adsorb, making the mineral form large aggregates.

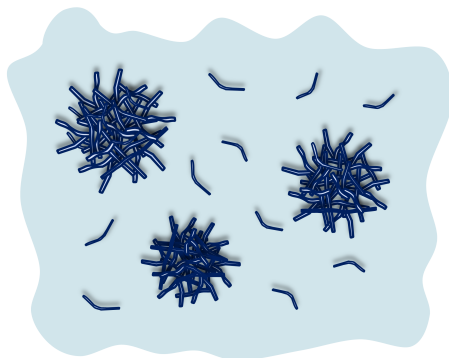

Schematic illustration of the organic colloids found in DOM.

This thesis provides new insight into the colloidal fraction of DOM, obtained with the use of scattering techniques. Our results show that colloidal structure may play an important role in stabilising DOM, and is thereby a factor which can affect long term carbon storage. We have a long way to go before we can accurately predict the fate of different carbon pools in different ecosystems, but hopefully these results add a valuable piece to the puzzle.

Populärvetenskaplig sammanfattning

Tänk dig en kolatom. I atmosfären förekommer denna som koldioxid och genom fotosyntes tas den upp av en växt och blir en del av ett blad. När hösten kommer faller detta blad till marken. Vilket öde som nu väntar vår kolatom beror på jordens nedbrytningsprocesser. Den skulle kunna omvandlas tillbaka till koldioxid inom några månader och återgå till atmosfären, eller så lagras den i jorden i hundratals år. Ungefär dubbelt så mycket kol som det finns i atmosfären och alla levande växter tillsammans lagras idag i marken. Vi vill gärna att det kolet stannar just i marken. För är det något vi lärt oss de senaste decennierna så är det att det har stora effekter på vårt klimat att rucka på balansen i kolcykeln.

Det är därför viktigt att vi förstår de mekanismer som kontrollerar lagringen av kol i jorden och andra ekosystem. Sådan kunskap kan hjälpa oss förbättra kolinlagringen och förutspå effekterna av ett förändrat klimat. Sådan kunskap är också viktig för jordbruk, jorderosion och dricksvattenkvalitet. Trots det kan vi fortfarande inte förklara vad som bestämmer ödet för vår kolatom.

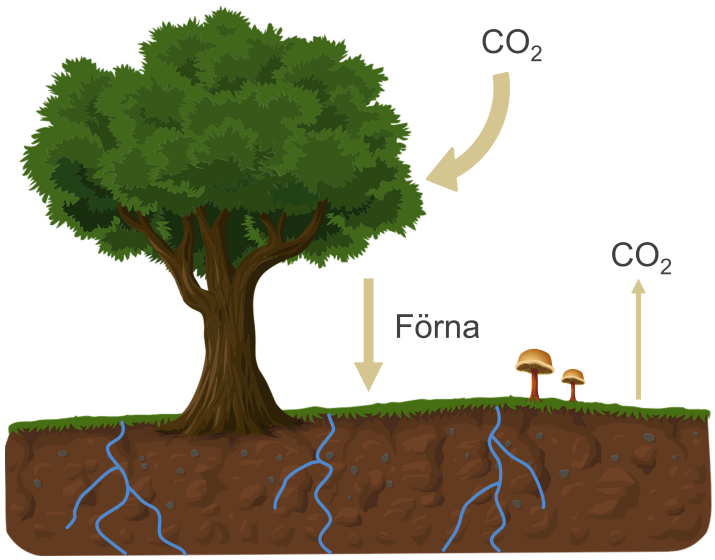

En förenklad bild av kolcykeln.

Döda organismer lämnar efter sig organiskt material. Detta material består till stor del av kol och bryts ner av olika mikrober så som bakterier och svampar, som på så sätt får tillgång till energi och näringsämnen. Den fraktion som anses vara lättast för mikrober att bryta ner är löst organiskt material, kallat DOM efter den engelska termen "dissolved organic matter". DOM är också ämnet för denna avhandling. Definitionen

av DOM är det organiska material i en vattenlösning som kan passera ett filter med en porstorlek på några hundra nanometer. Denna definition innebär att DOM är en blandning av många olika kemiska komponenter som kan variera i storlek, från små enskilda molekyler upp till stora partiklar som kallas kolloider.

Mycket forskning har ägnats åt att förstå den kemiska sammansättningen av DOM och hur denna påverkar DOM-nedbrytning och växelverkan med jordmineraler. Vi vet dock desto mindre om den fysiska strukturen hos DOM och detta gäller särskilt kolloiderna. Därmed vet vi inte heller hur struktur påverkar nedbrytning och växelverkan. Arbetet som beskrivs i denna avhandling har fokuserat på att karakterisera DOM, både kemiskt med hjälp av spektroskopi och strukturellt med hjälp av spridningstekniker. Denna kombination av tekniker innebär att vi kan erhålla information om DOM från små molekyler upp till kolloider. Lärdomarna från denna karakterisering användes sedan för att förstå bakteriell nedbrytning av DOM, samt vad som händer när DOM blandas med mineralpartiklar.

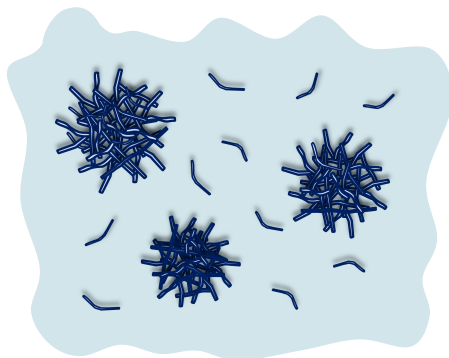

Illustration av kolloidalt DOM.

Vi har kommit fram till att DOM kemiskt främst består av kolhydrater, det vill säga stora sockermolekyler som bör utgöra en viktig energikälla för mikrober. Ungefär hälften av kolet i DOM är i kolloidal form och storleken och strukturen på dessa kolloider ändras beroende på de fysikaliska och kemiska betingelserna. Vid rumstemperatur observerade vi kompakta kluster men om temperaturen eller pH ökade fragmenterades dessa kluster till mindre delar. När DOM bröts ner av bakterier så förbrukades ungefär hälften av det organiska kolet men kolloiderna förblev intakta. När vi blandade DOM med mineralpartiklar observerades inte heller någon effekt på kolloiderna, medan små molekyler adsorberade och ledde till att mineralet bildade stora aggregat.

Denna avhandling ger nya insikter om den kolloidala fraktionen av DOM, vilka uppnåtts med hjälp av spridningsmetoder. Våra resultat visar att den kolloidala strukturen kan vara viktig för att stabilisera DOM och är därmed en faktor som kan påverka kolinlagring över långa tidshorisonter. Det återstår mycket jobb innan vi med säkerhet kan förutsäga hur olika kolreservoarer i naturen kommer utvecklas men förhoppningsvis kan dessa resultat bidra med några viktiga pusselbitar.

List of Publications

This thesis is based on the following publications, referred to by their Roman numerals:

I **Characterization of the Colloidal Properties of Dissolved Organic Matter From Forest Soil**

V. Meklesh, L. Gentile, **E. Andersson**, A. Bhattacharya, M. de Farias, M. Cardoso, H. Stålbrand, W. Loh, M. Skerlep, E. Kritzberg, A. Tunlid, U. Olsson, P. Persson
Front. Soil Sci., **2022**, 2:832706

II **Generation and properties of organic colloids extracted by water from the organic horizon of a boreal forest soil**

E. Andersson, V. Meklesh, L. Gentile, A. Bhattacharya, H. Stålbrand, A. Tunlid, P. Persson, U. Olsson
Geoderma, **2023**, 432:116386

III **The colloidal fraction of dissolved organic matter from forest soil persists microbial decomposition**

E. Andersson, M. Groeneveld, L. Tranvik, A. Tunlid, P. Persson, U. Olsson
Manuscript

IV **A contrast variation SANS and SAXS study of soil derived Dissolved Organic Matter, and its interactions with Hematite Nanoparticles**

E. Andersson, V. Meklesh, L. Gentile, R. Schweins, O. Matsarskaia, A. Tunlid, P. Persson, U. Olsson
Submitted

Publications not included in this thesis:

X-Ray Scattering Reveals Two Mechanisms of Cellulose Microfibril Degradation by Filamentous Fungi
D. Floudas, L. Gentile, **E. Andersson**, S. G. Kanellopoulos, A. Tunlid, P. Persson, U. Olsson
Appl. Environ. Microbiol., **2022**, 88, 17

Revisiting the Dissolution of Cellulose in NaOH as "Seen" by X-rays

B. Martin-Bertelsen, **E. Andersson**, T. Köhnke, A. Hedlund, L. Stigsson, U. Olsson
Polymers, **2020**, 12:342

My contributions to the papers

Paper I
I took part in sample preparation and data analysis and gave input on the manuscript.

Paper II
I designed the study together with my supervisors, performed sample preparation, NMR and scattering experiments. I analysed the data and wrote the manuscript with input from all co-authors.

Paper III
I designed the study together with my supervisors and performed all experimental work except elemental analysis. I analysed the data and wrote the manuscript with input from all co-authors.

Paper IV
I designed the study together with my supervisors and performed the sample preparation. I performed contrast variation SANS, SAXS and light scattering experiments, analysed the data and wrote the manuscript with input from all co-authors.

Abbreviations

cryo-TEM	cryogenic transmission electron microscopy
CP-MAS	cross-polarization magic-angle spinning
D_2O	deuterium oxide/heavy water
DLS	dynamic light scattering
DOM	dissolved organic matter
EPS	extracellular polymeric substances
Fe	iron
MOA	mineral-organic associations
NMR	nuclear magnetic resonance
OM	organic matter
P	phosphorus
PEG	polyethylene glycol
ppm	parts per million
SANS	small-angle neutron scattering
SAXS	small-angle X-ray scattering
SLD	scattering length density
SLS	static light scattering
SOM	soil organic matter
TN	total nitrogen
TOC	total organic carbon
WEOM	water extractable organic matter

Prologue

The work described in this thesis can be thought of as solving a puzzle with an unknown number of pieces. The picture slowly emerging, is that of dissolved organic matter (DOM) and its characteristics from the molecular to colloidal length scale. As these characteristics may influence the bioavailability and mobility of DOM, this picture can contribute to a deeper understanding of soil dynamics, as part of the carbon cycle, and of what factors that influence long term carbon storage in terrestrial and aquatic environments. The pieces put together so far were used to study the bacterial decomposition of DOM, and interactions between DOM and mineral particles.

We have studied DOM extracted from one soil type: the organic layer of a boreal spruce forest soil. From this work, the most important observations and conclusions are:

- DOM consists of both a low molecular weight fraction and a colloidal fraction. About half of the DOM carbon is present in the colloidal fraction.
- The dominating component of DOM is carbohydrates.
- The structure of colloidal DOM varies depending on extraction conditions.
- The larger size fraction of colloidal DOM is electrostatically stabilised.
- Colloidal DOM is resistant against bacterial decomposition, while the low molecular weight fraction is highly bioavailable.
- The low molecular weight fraction of DOM adsorb and induce aggregation and charge reversal of positively charged hematite particles.

1 Introduction

"You will die but the carbon will not; its career does not end with you."
– Jacob Bronowski

The title of this thesis is "Dissolved Organic Matter from a colloidal perspective". Throughout this thesis, I will justify why this perspective is important to consider, but first I would like to explain the two concepts comprising the title. If we start with the second part: Colloids are generally described as particles in solid, liquid or gaseous phase, having at least one dimension ranging between 1–1000 nm, which are dispersed in a continuous medium that in turn also can be solid, liquid or gas[1,2]. Some examples of colloidal systems are paints, milk, detergents, cosmetics, smoke, blood and, to some degree, soil. Constituting the border between molecules and bulk phase systems, the study of colloids requires its own techniques and theories, as you will see throughout this book.

Now, let us move over to dissolved organic matter.

1.1 Soil, organic matter and the carbon cycle

We all have a relation to soil, yet few people have a clear perception of what soil is. In 1998, the International Union of Soil Sciences defined soil as[3]

> *"...a continuous natural body which has three spatial and one temporal dimension... It is formed by mineral and organic constituents and includes solid, liquid and gaseous phases... Study of the structures of the soil cover facilitates perception of the physical, chemical and biological properties; it permits understanding the past and present of the soil, and predicting its future."*

This is a complex definition, reflecting the complexity of soil, but it highlights some key features that will be important throughout this book. It tells us that soil contains both organic and inorganic components, which can be solid, liquid or gas, and which have both physical, chemical and biological properties. It also highlights the aspect of time, and our quest for understanding the fate of soils.

Studying and understanding soil is becoming increasingly important. Soil constitutes a large part of our physical world and a provider of major resources, unfortunately becoming extensively depleted[4,5]. In recent decades, the ability of soil to store carbon, and the general role of soil in the carbon cycle, has gained a lot of interest due to the urgency of climate change. It has been estimated that soil is storing twice as much carbon as the atmosphere and all living plants combined[6], and the largest carbon reservoir in terrestrial ecosystems is soil organic matter (SOM)[7-9]. Organic matter (OM) is in principal the remains of all living things. OM constitutes carbon based compounds which through decomposition are turned into nutrients and a source of energy for new biomass production. That the dynamics of SOM carbon remains

stable is central for the balance of the carbon cycle and thus for the climate and our society[10-12]. This means that the time between OM entering the soil and respiration of the carbon as CO_2 back to the atmosphere should not decrease, but preferable increase. The same is true for aquatic systems, which also store large amounts of carbon[13]. Understanding of the mechanisms controlling storage and decomposition of carbon is therefore of high importance. Such knowledge would be beneficial for predicting the effects of a changing climate and improving estimates of carbon fluxes used in climate models[13-16], as well as for developing farming strategies, preventing soil erosion, optimising carbon sequestration[4,6,17,18] and retaining good drinking water quality[19,20]. However, reaching this level of understanding has proven as complex as the soil itself.

1.1.1 Organic matter decomposition

So why does soil contain so much carbon? Why is not all OM quickly respired back into CO_2? Well, this is actually still not understood[21,22]. The main decomposers in soil and water systems are bacteria and fungi[14,22,23]. These species "eat" by absorbing nutrients over the cell membrane, which requires a water environment and molecules of a suitable size[24,25]. To obtain such nutrients, microbes secrete various enzymes that are able to cleave chemical bonds in larger molecules[25,26]. OM has generally been considered to consist of two different fractions, one labile fraction which is quickly mineralised by microbes, and one stable or recalcitrant fraction which appears to persist for millennia[7,9,10,14]. It is however widely debated, in both the soil and aquatic communities, what distinguishes the two fractions, and if OM should at all be divided into two such fractions[11,21,27]. There are two main views of what determines the stability of OM, one focusing on intrinsic or chemical factors, and one focusing on extrinsic or physical factors.

1.1.1.1 Intrinsic factors

Historically, there has been a large focus on how the molecular composition or "substrate quality" relate to the decomposition of OM. Studying the SOM fraction directly in the intact soil is hard, because of the complexity described above, and therefore SOM is usually extracted from the soil[28-30].

The traditional extraction method when studying SOM has been to use alkaline solvents, in recent times mainly NaOH[31], followed by different steps of acidification[10]. This process originates from when Francois Charles Achard studied peat in 1786, and concluded that the extraction yield was highest when using strong base[10,32].

Since then, standardised procedures have been developed and different SOM fractions such as humic acid (soluble above pH 2), fulvic acid (soluble at all pH conditions) and humin (water insoluble) have been operationally defined and thoroughly investigated[33-36]. Humic substances are generally considered to constitute a stable fraction of SOM and are described as complex high molecular weight aromatic substances formed during microbial degradation[10,11,37]. Some studies suggests however that humic substances consists of a mixture of known biopolymers and not a chemically distinct fraction[38,39]. In the last decades, there has been a growing debate about to what extent the alkaline extractions recover the intact OM present in soils[9,11,31].

Putting humic substances aside, substrate quality in relation to microbial OM decomposition can still be evaluated in terms of chemical properties[40-42]. Such properties are for example: size, as only small molecules can be directly absorbed without further processing; types of chemical bonds in the structure, aromatic double bonds are e.g. harder to break than ester linkages; irregularity of the chemical structure, as highly irregular structures, like lignin, requires non-specific enzymes; hydrophobicity, as this will affect the dissolution and passage over the cell membrane; toxicity to microbes and content of specific nutrients[43-45]. Based on these different characteristics, litter components are generally considered decreasingly labile in the order from monosugars, amino acids and small organic acids, to cellulose and hemicellulose, and further to aliphatic and aromatic compounds such as cutin and lignin[40,43,45,46]. However, it has been shown that also compounds considered non-labile can indeed be decomposed under the right conditions[9,47].

1.1.1.2 Extrinsic factors

As mentioned above, microbial uptake has some requirements. If these are not fulfilled, even a precious monosaccharide will escape decomposition. Extrinsic factors affecting decomposition can for example be access to moisture, oxygen levels, pH and a suitable temperature for microbial activity[25,48-52]. Apart from this, adsorption onto mineral surfaces, and the formation of mineral-organic associations (MOA), is considered a major factor stabilising OM[9,22,48,53-55]. The reduced bioavailability could be due to several different mechanisms such as decreased enzyme efficiency when functional groups of the OM are bound to minerals, conformational changes of the OM leading to decreased enzyme recognition or that the enzymes themselves adsorb[53,56,57]. The reduced bioavailability could also be a direct effect of decreased solubility and diffusion of the OM[45]. There are however studies indicating that OM in direct association with a mineral surface may still be decomposed without desorption[58-60]. In aquatic systems, formation of MOA is often related to increased sedimentation and burial of OM in sediments[61,62], but it may also stabilise the minerals

in solution, leading to increased mineral transport and water browning[20,63,64]. Stabilisation by formation of MOA will in the long run be an effect of adsorption affinity and preferential adsorption of high molecular weight fractions, hydrophobic fractions, aromatic fractions and carboxylic fractions has been reported[53,65-70]. This relates back to the intrinsic properties of OM discussed above.

Another factor considered important for the stabilisation of SOM is the formation of soil aggregates[17,71-73]. Soil has structure on the cm to nm length scale and contains both macro ($>$ 250µm) and micro ($<$ 250µm) aggregates with varying degrees of porosity[74-76]. These aggregates can contain OM, microbes and minerals such as clay or different oxides[75]. The stabilisation by aggregation is attributed to a physical separation between OM on the inside of aggregates, and microbes excluded due to there physical size[77]. Also, narrow pores limits the diffusion of water and oxygen inside the aggregates[77,78].

The importance of extrinsic factors is currently being emphasised within soil science[9,11,22], while in the aquatic sciences there is still a strong focus on intrinsic factors[79-81]. This discrepancy between different fields of research makes it clear that the factors controlling the biodegradability of OM, are not well understood[21].

1.2 Dissolved Organic Matter

Because of the requirements for decomposition described above, dissolved organic matter (DOM) is considered the most bioavailable fraction of OM[45,52]. This fraction, although constituting only a few percent of the total OM carbon in soils[82], is also important because of its mobility. High mobility means it can act as a vector for nutrients and contaminants, and connects the terrestrial and aquatic environments[29,58,82-86]. In aquatic systems, DOM constitutes the major carbon pool, of a total size similar to atmospheric carbon[87-89]. DOM is also the fraction relevant for formation of MOA[65].

DOM is operationally defined as the OM fraction in a solution which is not retained upon filtration. The filter size used is normally around 0.45µm but can vary from 0.2 to 0.7µm[29,82,89,90]. This definition implies that DOM contains a chemical and structural mixture of components, on a wide size scale from low molecular weight molecules up to colloids. In the study of DOM, this comprise an aggravating fact, as different analysis techniques tend to be sensitive to specific size classes.

The operational definition also means that DOM can be obtained in several different ways, each entailing its own possible artefacts[85,89,90]. Aquatic DOM may be sampled directly from streams, lakes or the ocean and then filtered in a suitable way[89]. But

how does one obtain the solution phase of soil? Methods used in the literature includes lysimeters[29,91,92], containers installed in the soil which collect water at a certain depth by e.g. suction; centrifugation[86] of collected field-moist soil, and lab extractions of soil[29,85,90]. Although lysimeter sampling is considered an *in situ* method, obtaining large enough sample volumes can be difficult, depending on the soil and weather conditions[29]. Lab based extractions are therefore often more reliable and frequently used. The extraction procedures may differ, using either water or dilute salt solutions, different extraction times, different temperatures and varying degrees of shaking or stirring[30,85,86,93]. The obtained material is sometimes referred to as water extractable organic matter (WEOM), however we will throughout this book use the term DOM regardless of the method used. The effect of different extraction procedures has been thoroughly investigated in terms of chemical differences and extracted concentrations. Generally the concentration of DOM increase with increasing extraction time, temperature and agitation[85,94-97]. However, not much is known about the effects on structure and the colloidal DOM.

DOM colloids are suggested to contain a large fraction of the DOM carbon[83,91]. Despite the importance of DOM in both terrestrial and aquatic ecosystems described above, our understanding of DOM decomposition and adsorption processes, is limited by a lack of knowledge about DOM structure and dynamics at the colloidal length scales. This means we are missing an important piece of the puzzle in our understanding of the carbon cycle.

1.3 This thesis

The work described in this thesis has focused on connecting structural information about colloidal DOM, covering a wide size range, with chemical information, by using a multi-method approach for analysis. The studied DOM was extracted by water from the organic layer of a boreal spruce forest soil.

The samples and main characterisation techniques used are first described in Chapters 2 and 3. Then, Chapter 4, describes the main results and conclusions from the chemical and structural characterisation of DOM, obtained by comparing different extraction procedures. In Chapter 5, we investigate how the colloidal size and structure affect bacterial decomposition of DOM. Finally, in Chapter 6, we have studied DOM interactions with mineral particles.

2 Materials

The sampling location for most of the soil samples, a Norway Spruce forest planted 1957 at Tönnersjöheden Experimental Forest.

In this chapter, the materials and processes used to produce samples for the experimental studies are described.

2.1 Soil

Soil samples were collected at Tönnersjöheden Experimental Forest close to Simlångsdalen in Halland, south west Sweden (Figure 2.1 A), an area with maritime temperate climate. Tönnersjöheden was founded 1923 and is operated by the Swedish University of Agricultural Sciences[98]. The sampling location consists of first-generation Norway spruce (*Picea abies*) forest planted on previous agricultural land or heathland. The soils in the area are classified as Arenosols[92], meaning they have a texture of loamy sand or coarser, low water-holding capacity and low nutrient content[3]. The ground vegetation is dominated by moss. For Paper I, samples were collected from a chronosequence of forest stands planted 1983, 1957 and 1928, and adjacent fields as reference plots. For Papers II-IV, soil was collected from the forest planted 1957.

Soil is divided into different horizons or layers based on physical, chemical, and biological characteristics[3]. The surface layer is the organic horizon (O) which is rich in organic matter. The depth of the O-horizon depends on litter input, providing fresh OM, and the rate of OM decomposition. Beneath the O-horizon there is the mineral soil which can be divided into topsoil (A), subsoil (B), the parent material (C) and bedrock (R)[99]. Depending on which classification system is used, additional horizons and variations in naming occur. The fraction of OM decreases and the inorganic fraction increases with soil depth.

Soil profiles were dug up using a spade and the organic layer (including the litter layer), ending where the soil changed color to darker brown/grey, was sampled (Figure 2.1 B). The surface cover of plant material was removed. The depth of the organic layer increased with the stand age of the forest, meaning a steady state for the establishment of the organic layer was not reached after 60–90 years. The soil was sieved through a 2 mm sieve to remove roots, animals and stones and obtain homogeneous samples. The sieved soil was kept field moist and stored dark at 4°C in sealed plastic bags.

2.2 Soil extracts

DOM was extracted from the soil samples. Different extraction protocols were used and assessed throughout this work (see Papers I-II) but here the general procedure is described.

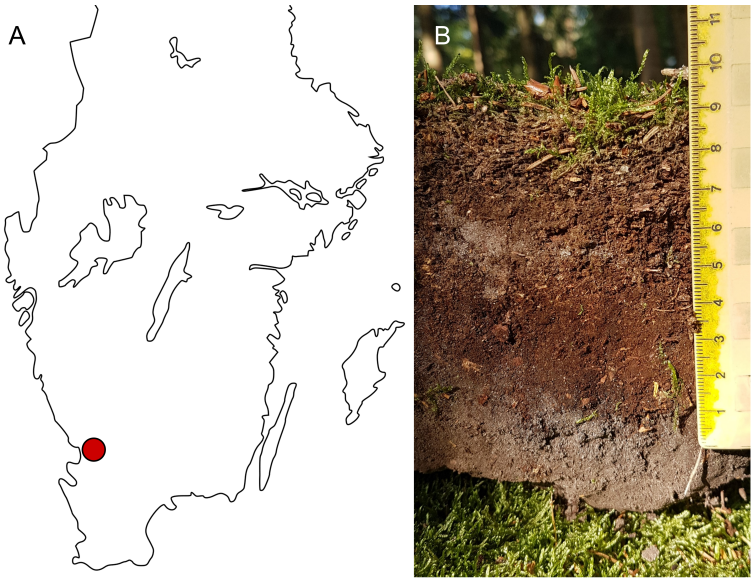

Figure 2.1 A) The red dot mark the sampling location, Tönnersjöheden Experimental Forest in south west Sweden. B) Soil profile from the forest planted 1957. For soil samples, the organic layer was used, representing ca. 1–8 cm in this figure.

Soil and water were mixed in a ratio of 1:5 weight to volume, using magnetic stirring or shaking. Extractions were carried out at different temperatures and for varying times, after which the soil slurry was pressed by hand through a nylon mesh of 150 µm pore size and centrifuged at 1700 g for 5 min to remove the solid fraction. The supernatant was filtered through glass microfibre filters of 2.6, 1.6 and finally 0.7 µm pore size using suction filtration. Finally, the solution was filtered through sterile polyethersulfone syringe filters with a pore size of 0.2 µm, into sterile plastic tubes. This step was carried out in a clean bench. The liquid volume recovery was generally around 70%. A pore size of 0.2 µm was chosen in favour of 0.45 µm mainly to reduce the microbial content as much as possible, to obtain samples which could be stored and studied for longer periods of time.

2.3 Hematite

As a model system for studying DOM-mineral particle interactions (Paper IV), hematite nanoparticles were synthesised. Hematite (α-Fe_2O_3) is one of the thermodynamically most stable forms of iron oxide under aerobic conditions, and it is therefore widespread in natural soils[100]. Hematite nanoparticles were synthesised by forced hydrolysis according to the procedure of Schwertmann and Cornell[100]. 0.002M HNO_3

was heated to 98°C and unhydrolysed crystals of $Fe(NO_3)_3 \cdot 9\ H_2O$ were added under vigorous stirring to a concentration of 0.02M Fe. The solution was kept in an oven at 98°C for a week after which the formed particles were centrifuged and washed. The final hematite solution had a pH of 4.5 and was stored at 4°C in plastic tubes.

For neutron scattering experiments, with the intent to control the neutron contrast, the H_2O solvent was exchanged for either 100% D_2O or 30% D_2O. This was done by centrifugation, exchange of the supernatant to pH adjusted (pH 5.5) D_2O or 30% D_2O, and redispersion of the particles. The procedure was repeated 4 times. The pH=5.5 was chosen to match that of the DOM extracts used in the study.

The hematite product was confirmed by powder X-ray diffraction[101] (Figure 2.2 A) and the synthesised particles had a surface area of 53 m^2/g as determined from Brunauer-Emmett-Teller (BET) analysis, using N_2 as adsorption species. Transmission electron microscopy (TEM) showed a rhombohedral particle shape, with a side length around 25 nm (Figure 2.2 B). This shape and size of the product has been observed previously from similar synthesis[102,103]. However, by the use of cryo-TEM (see Section 3.2.2) we discovered that the hematite particles were partially aggregated into clusters with a size of around 100-200 nm (Figure 2.2 C). Further details on the characterisation of the hematite are found in Chapter 6 and Paper IV.

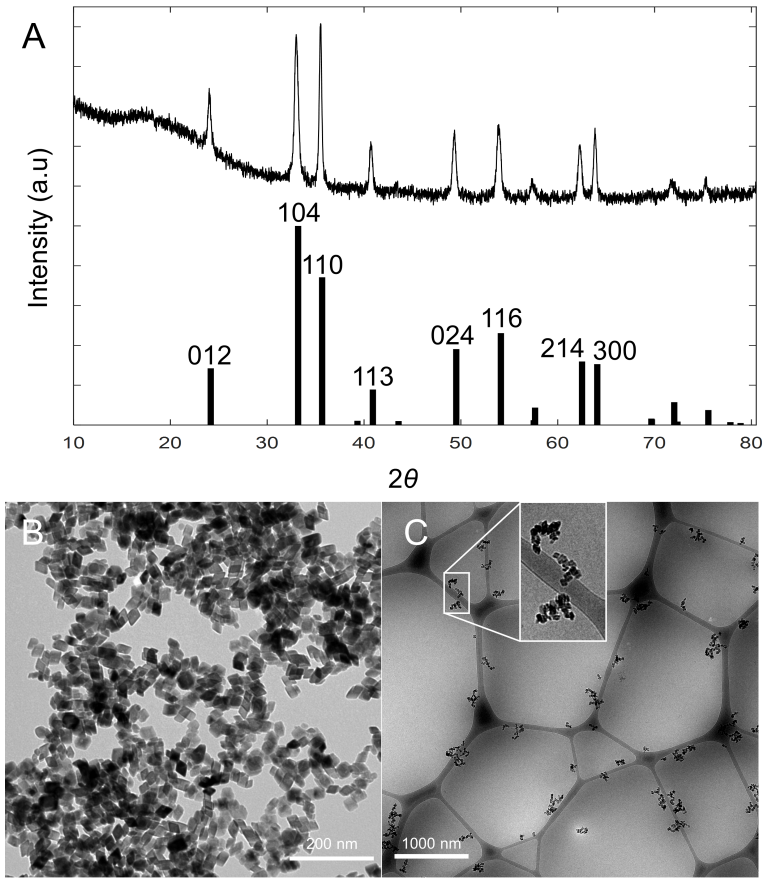

Figure 2.2 A) Powder X-ray diffraction pattern of the synthesised hematite compared with a theoretical reference pattern where Miller indices (hkl) are indicated. B) TEM image of synthesised hematite nanoparticles dried on a surface. The scale bar represents 200 nm. C) Cryo-TEM image of the hematite aggregates with an inset showing a close up of the marked area (345 x 565 nm). The hematite solution had a concentration of 50 mg/l. The scale bar represent 1000 nm.

3 Methods

"The real voyage of discovery consists not in seeking new landscapes, but in having new eyes."
– Marcel Proust

In this chapter we introduce the experimental methods used in the studies presented in this thesis. We conclude that a combination of several different experimental techniques are indeed necessary to understand the different aspects of DOM. In particular we acknowledge that a detailed chemical characterisation is a prerequisite to properly analyse the scattering data of colloidal DOM.

The chemical characterisation of DOM (Section 3.1) included (i) elemental analysis; (ii) pH; (iii) monosugar composition; (iv) infrared spectroscopy (IR); (v) solid-state ^{13}C nuclear magnetic resonance (NMR) and (vi) solution ^{1}H NMR. For more information about (iii) and (iv), see the methods section of Paper I. Structural information on the colloidal length scale (Section 3.2) was obtained using different scattering methods (visible light, X-ray and neutron scattering), in addition to cryogenic transmission electron microscopy (cryo-TEM). For the study of hematite particles and bacteria, standard TEM and light microscopy respectively were also used. The colloidal stability was assessed through electrical charge by the zeta potential (Section 3.3). Figure 3.1 presents an overview of the methods used when characterising DOM, and the main information they provide.

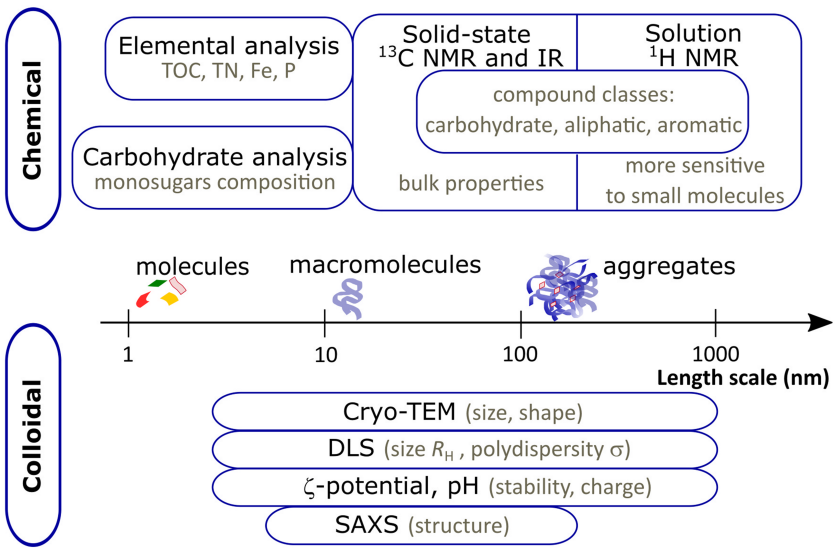

Figure 3.1 Summery of the methods used to characterise chemical and colloidal properties of DOM, and the respective information obtained. The length scale applies to the colloidal characterisation methods in the lower part of the figure. SLS and SANS are not included in the figure, which is taken from Paper I.

3.1 Chemical characterisation

3.1.1 Elemental analysis

The concentrations of total organic carbon (TOC), total nitrogen (TN), iron (Fe) and phosphorus (P) in our soil extracts were determined by elemental analysis. There are several methods in use for these kinds of analysis. Here we shortly describe the specific ones used in this work.

TOC and TN were quantified by combustion, after the inorganic carbon fraction had been removed by acidification. The amount of CO_2 produced was quantified by non-dispersive infrared analysis and the nitrogen oxides by chemoluminescence. A common quantity to measure in the study of DOM (sometimes used interchangeably) is dissolved organic carbon (DOC), defined as the organic carbon in solution after filtration, usually through 0.45 µm filters although other sizes are used[104]. As all our extracts are initially filtered through 0.2 µm filters, the organic carbon fraction could classify as DOC. However, we use the term TOC throughout this work to highlight that we quantify all organic carbon present in the samples at the time of analysis, including material which may have aggregated.

Fe and P were quantified using Inductively Coupled Plasma Optical Emission Spectrometry (ICP-OES). In this technique, plasma is used to excite the electrons in an injected liquid sample. As the electrons relax back to their original state, light is emitted at wavelengths characteristic for the specific element, and the emission intensity is proportional to the concentration of that element[105]. By this technique it is also possible to assess many other types of trace elements[106], which were not considered in this work.

3.1.2 Nuclear Magnetic Resonance

Nuclear magnetic resonance (NMR) is a radiofrequency spectroscopy technique, that can provide information about the atomic composition of molecules and the chemical environment of specific nuclei[107,108]. It is commonly used to determine the chemical structure of organic compounds. NMR builds on the principle that atomic nuclei posses a nuclear spin (if the mass number of the nuclei is odd) giving rise to a magnetic moment. The following short description will only cover spin ½ nuclei such as ^{1}H or ^{13}C, where the spin can acquire two possible orientations in an external magnetic field $\overline{B}_0$. In the absence of an external field, the spins are randomly oriented and the magnetic moments cancel out. The two possible orientations are either alignment parallel with the field, which is a lower energy state α, or antiparallel, which is a

higher energy state β (Figure 3.2). The energy difference between the two spin states depends on the gyromagnetic ratio, γ, of the nuclei, and is given by

$$\Delta E = \frac{h\gamma \left|\overline{B}_0\right|}{2\pi} \tag{3.1}$$

where h is Planck's constant. It follows from Eq. 3.1 that the stronger the magnetic field, the smaller energy differences we can resolve.

In an NMR experiment, a short radio frequency pulse is applied over the sample, giving rise to a magnetic field oscillating at a frequency $\nu = E/h$. If the frequency matches ΔE, it is called a resonance frequency and the energy will be absorbed promoting spin flips from α to β. Electrons surrounding the nucleus shields it from the magnetic field, giving rise to a change of the resonance frequency. This is accounted for by a local correction of Eq. 3.1 called the chemical shift. The chemical shift depends on the local chemical environment and results in a spectrum allowing for chemical recognition. An NMR spectrum shows absorption as a function of chemical shift expressed as parts per million (ppm). The energy absorption is proportional to the number of nuclei coming into resonance, meaning the NMR signal is quantitative.

In this work we have used two different NMR techniques. Firstly, solution ^{1}H NMR was used to analyse mainly the low molecular weight fraction of DOM, using excitation sculpting with water suppression to remove the very strong signal of the solvent[109]. In solution NMR, the linewidth depends on the rotational dynamics of the detected species and freely tumbling molecules will result in narrow peaks in the spectrum. Large components on the other hand tumble slowly and give broad peaks.

For quantification, we constructed a calibration curve based on an external standard of polyethylene glycol (PEG), as shown in Figure 3.2. To convert from integral area of an NMR peak to the concentration of that component, the chemical formula of the component has to be known.

Secondly, cross-polarization magic-angle spinning[110] (CP-MAS) solid state ^{13}C NMR was used on freeze dried samples, to obtain the bulk composition. CP enhances the signal from the isotopically dilute ^{13}C nuclei and MAS improves the spectral resolution by simulating the motional averaging that occurs in liquid samples.

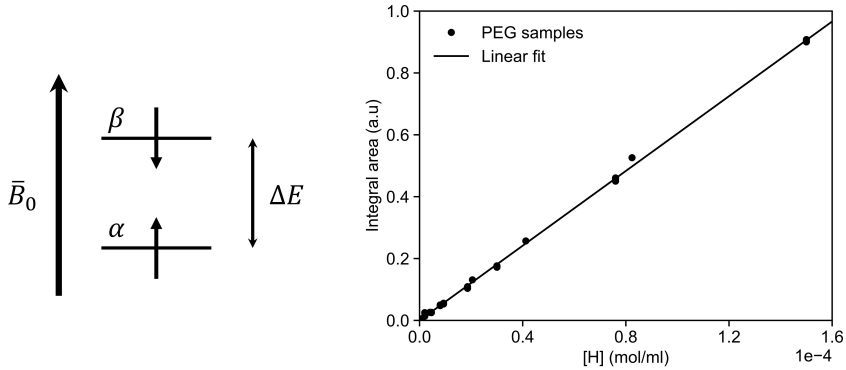

Figure 3.2 Left: Schematic illustration of the two spin states for a spin ½ nuclei, after alignment in an external magnetic field $\bar{B}_0$. Right: Calibration curve for quantification of the NMR signal, constructed from measurements of PEG using water suppression.

3.2 Structural characterisation

3.2.1 Scattering methods

Scattering techniques allows us to determine colloidal structure and interactions in solution, and they are widely applied in studies of soft matter[111-113]. They are based on the principle that when irradiating a sample, the radiation can either be transmitted, absorbed or scattered, i.e. change direction. The scattered radiation carry information such as size, structure and dynamic behaviour of the scattering object. As different types of radiation covering different wavelengths can be used, such as visible light, X-rays or neutrons, length scales from one to several hundred nanometres can be probed. Scattering techniques are also generally non-invasive, requires very little sample preparation and can be performed on liquid or solid samples. The information obtained correspond to bulk properties of the sample, as the detected signal is an average over all objects and orientations in the radiated sample volume. These properties make scattering complementary to imaging techniques. However, in order to obtain useful scattering data, a well collimated beam is necessary. Also, if having polydisperse samples, large scattering objects will dominate the signal, making it hard to obtain information about other size fractions in the sample.

In this work, the techniques used were static light scattering (SLS) and dynamic light scattering (DLS), small-angle X-ray scattering (SAXS) and small-angle neutron scattering (SANS).

3.2.1.1 Static Scattering

In a scattering experiment, such as schematically illustrated in Figure 3.3, the incident radiation can be described as a planar wave with a wave vector of magnitude $|\bar{k}_0| = 2\pi/\lambda$, where λ is the wavelength. An elastic scattering event with a point scatterer results in a spherical wave with wave vector magnitude $|\bar{k}_s| = |\bar{k}_0|$. Elastic scattering means that the energy is conserved, such that λ remains unchanged, and throughout this book we will assume elastic scattering. We also assume that the spherical wave is formed instantaneously meaning that the planar and spherical waves are in phase, referred to as coherent scattering, and that the incoming radiation is only scattered once before detection. There will be a phase difference between the spherical waves produced from different scattering events distributed in space, due to the path length distance at detection. This leads to constructive or destructive interference depending on the scattering angle θ (Figure 3.3). In practice, one works with the so called scattering vector $\bar{q} \equiv \bar{k}_s - \bar{k}_0$ which describes the momentum transfer of the scattering event and, as derived from the scattering geometry (Figure 3.3), has the magnitude

$$|\bar{q}| = q = \frac{4\pi}{\lambda} \sin \frac{\theta}{2} \tag{3.2}$$

As q contains both the scattering angle and wavelength, it becomes a practical parameter when comparing data between different experimental set-ups and radiation sources used. q has the unit of length^{-1} meaning we work in reciprocal space, such that small values of q (small scattering angles) relate to large structural features in the sample and vice versa. A scattering experiment covering a q-range of $q_{\min} - q_{\max}$ will probe structures on the length scale of approximately $1/q_{\max} - 1/q_{\min}$. To access smaller features in a sample, one can either use a shorter wavelength, or detect wider angles by decreasing the sample to detector distance or use a larger detector, all will result in an increased q-value.

The probability of a scattering event is described by the scattering length b, which will vary depending on the type of atom and the radiation used (see Section 3.2.1.2). b can be thought of as the cross section of a target, larger cross section means higher probability of hitting, i.e. scattering. The amplitude of the scattering from N atoms in vacuum, at positions r_j becomes[111]

$$A(\bar{q}) = \sum_{j=1}^{N} b_j e^{-i\bar{q}\cdot\bar{r}_j} \tag{3.3}$$

where $e^{-i\bar{q}\cdot\bar{r}_j} = \cos qr_j + i \sin qr_j$ describes a complex wave. In a real sample, the scattering objects (particles) consists of many atoms and are surrounded by a medium. When this is the case, and the length scale probed is much larger than the distance

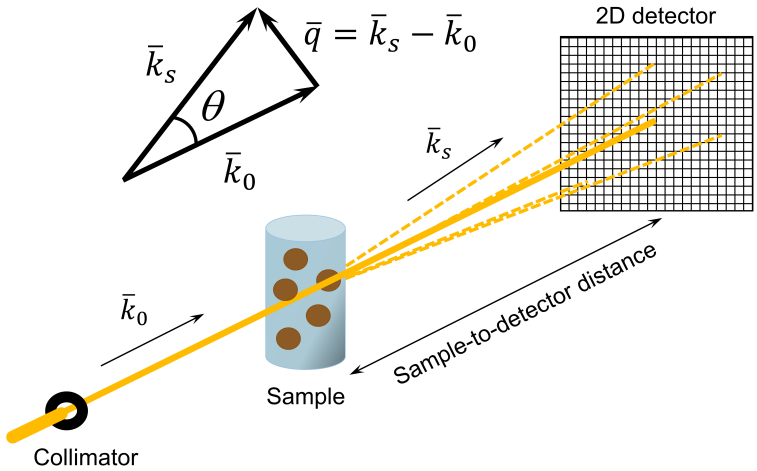

Figure 3.3 Schematic illustration of a scattering experiment and the geometry defining the scattering angle θ and scattering vector ***q***.

between atoms, as in small-angle scattering, it is convenient to go from a discrete to a continuum description such that

$$A(\bar{q}) = \int_V \rho(\bar{r}) e^{-i\bar{q}\cdot\bar{r}}\, d\bar{r} \tag{3.4}$$

where the integral is over the whole irradiated sample volume V and $\rho(\bar{r})$ is the scattering length density (SLD), describing the density of b over V. Eq. 3.4 is the Fourier transform of the scattering length density distribution.

The measurable quantity in a scattering experiment is the intensity $I(q) = |A(q)|^2$, meaning the phase information is lost. Eq. 3.4 shows that the scattered intensity actually arises because of inhomogeneities in the scattering length density[111]. Over time, we collect the scattering from many particles at different locations in space, having different orientations, meaning our experimental *I(q)* reflects a time and spatial average.

The coherent, elastic, scattering intensity of particles in a solution can generally be expressed

$$I(q) = \phi_p V_p \Delta\rho^2 P(q) S(q) \tag{3.5}$$

where ϕ_p is the volume fraction of particles in the sample, V_p is the particle volume and $\Delta\rho = \rho_{particle} - \rho_{solvent}$ is the SLD difference between the particles and the solvent. $\Delta\rho$ describes the contrast between different parts of the sample (see Section 3.2.1.2). For composite particles having internal structure with domains of different ρ_j, $\rho_{particle}$ becomes the volume average SLD of the different domains. *P(q)* is the single particle

form factor, a function containing information about the size and structure of the scattering particle. The structure factor *S(q)*, describes how the scattering is affected by interactions between particles. Under dilute conditions, inter particle interactions can be neglected and $S(q) = 1$. Throughout this book we assume dilute conditions. We will mainly use Eq. 3.5 with the first two terms expressed as cM/d^2N_A, where c is the concentration of particles (in mass per unit volume), M is the particle molecular weight, d is the mass density of the particles and N_A is Avogadro's constant.

3.2.1.2 Visible light, X-rays or neutrons

As in imaging, contrast is a key parameter determining what we can actually see in a scattering experiment. If the SLD of our scattering objects is similar to that of the solvent, $\Delta\rho \approx 0$ and $I(q) \approx 0$ according to Eq. 3.5. The scattering length of a material depends on how the radiation interacts with the atom.

In light scattering, the interaction occurs with the electron cloud. A dipole moment is induced by the electric field of the incoming radiation, and the strength of the interaction will depend on the polarizability of the scattering material. The polarizability is in turn $\propto n^2$, the refractive index of the material[111,112]. X-rays are also scattered by interactions with electrons, but here the scattering length scales proportionally with the number of electrons in the electron cloud, since the energy is high enough for every atom to act as an individual scattering centre[112]. This means that materials with higher atomic number will scatter X-rays more strongly. While this can be convenient in studies of metals, it poses a problem when you are interested in organic materials consisting mainly of hydrogen, oxygen and carbon. Their scattering signal may be completely covered by the scattering of heavier atoms. A possible solution in this case is to use neutrons[114]. They are instead scattered by interactions with the nucleus of an atom and the scattering length varies randomly over the periodic table. The scattering length for neutrons can be both positive and negative, and also depend on the isotope. Of particular use is the large difference in scattering length between hydrogen and deuterium. As H_2O ($\rho = -0.56 \times 10^{10}\text{cm}^{-2}$) is a commonly used solvent with similar properties as D_2O ($\rho = 6.39 \times 10^{10}\text{cm}^{-2}$), one can in many systems adjust the contrast between the solvent and particles in the sample by mixing H_2O and D_2O in different ratios[115]. This technique is called contrast matching and is useful when you study a multicomponent system where the components have different SLDs. By matching the SLD of the solvent with one of the components, this component becomes practically invisible and the scattering pattern will only contain information about the non-matched component(s). This is schematically illustrated in Figure 3.4 for the case of DOM and hematite particles.

For a system containing one kind of homogeneous particle (such that only one con-

trast is involved), *I(q)* obtained by one type of radiation can be rescaled to the contrast of a different type of radiation, by the ratio between the optical constants. This is for example described by Martin-Bertelsen et al.[116] in the case of scaling SLS data to SAXS intensity. In this way, the q-range can be widen by combining data obtained with radiation of widely different wavelengths.

Figure 3.4 Schematic illustration of neutron contrast matching for DOM and hematite. The different colours represent different SLDs.

3.2.1.3 Dynamic scattering

In this work, dynamic scattering was mainly used for particle sizing. While static scattering uses the angular dependence of scattered intensity averaged over time, dynamic scattering probes time-dependent intensity fluctuations due to Brownian motion of particles[113]. This can be done at one or several scattering angles. The interference pattern captured on a 2D detector at a single time point is called a "speckle pattern" and as particles move with time, the phase of scattered waves will change, as will the speckle pattern. By tracking the scattered intensity at a certain scattering angle in time, one can obtain information about the mobility of the particles. This is expressed as the normalised intensity autocorrelation function[111]

$$g_2(q,\tau) = \frac{\langle I(q,0)I(q,\tau)\rangle}{\langle I(q)\rangle^2} \tag{3.6}$$

where *I(q,0)* is the scattering intensity at time 0, $I(q,\tau)$ is the intensity after a time step τ, and $\langle I(q)\rangle$ is the time-averaged scattering intensity. At short time intervals, before the particles have moved, the correlation is equal to 1 and with time it decays down to 0.

The information we want to obtain is contained in the field autocorrelation function $g_1(q,\tau)$, which is related to $g_2(q,\tau)$ by the Siegert relation[117]

$$g_2(q,\tau) = 1 + \beta[g_1(q,\tau)]^2 \tag{3.7}$$

where β is a system dependent correction factor. For a system of non-interacting polydisperse colloids, $g_1(q,\tau)$ will be a sum of exponentials, one exponential for each size species. The average diffusion coefficient $\langle D \rangle$ of the colloids can then be obtained from a cumulant expansion as[113]

$$g_1(q,\tau) = e^{-\langle\Gamma\rangle\tau}[\,1 + \frac{\sigma}{2}\langle\Gamma\rangle^2\tau^2 + ...] \tag{3.8}$$

where $\langle\Gamma\rangle = q^2\langle D\rangle$ is the average decay rate of the exponentials and σ is the relative variance of Γ referred to as the polydispersity index (PDI). At low values of q, the z-averaged hydrodynamic radius $\langle R_H \rangle$ can be obtained from the average diffusion coefficient using the Stokes-Einstein relation

$$\langle D \rangle = \frac{k_B T}{6\pi\eta\langle R_H\rangle} \tag{3.9}$$

where k_B is Boltzmann's constant, T is the temperature and η is the viscosity of the solvent.

The hydrodynamic radius describes the radius of a theoretical hard sphere, diffusing at the same rate as the observed colloid. The z-average is an intensity weighted average and since scattered intensity scales with the square of the particle volume, $\langle R_H \rangle$ will be strongly biased towards the largest species in a sample. See also the discussion in section S2.1 in the supplementary material of Paper I.

3.2.2 Cryo-TEM

Transmission electron microscopy (TEM) is an imaging technique where a beam of electrons is used instead of light. The short wavelength of the electrons make it possible to resolve structures down to sub-nm length scales[118]. As revealed by the name, the image is formed by electrons transmitted through the sample, providing a 2D projection. For non-crystalline materials, the contrast is defined by how well the material scatters electrons, meaning it scales with the atomic number. As discussed also in Section 3.2.1.2, this can be a problem when studying organic materials. As a further complication, the sample is usually deposited on a carbon coated grid.

Standard TEM is performed in vacuum and the sample needs to be fixated to the grid by, for example, drying. This poses a problem in the study of biological and soft matter systems as the fixation may jeopardize the integrity of the sample structure and cause aggregation. The solution to this problem is cryogenic-TEM (cryo-TEM)[119, 120], where the sample is instead vitrified, i.e. frozen very quickly without formation of ice crystals (although this is hard to achieve in practice). The vitrified sample will more closely resemble the structures in the solution state and provides a snap-shot of

the otherwise dynamic system. As with all imaging techniques, the field of view is limited and it is hard to know if what is seen in one image is representative of the whole sample.

3.3 Colloidal stability

For colloidal size particles in solution, Van der Waals interactions are typically not negligible and the particles need to be stabilised to avoid aggregation. The two main stabilisation mechanisms in colloidal systems are electrostatic stabilisation, arising from surface charges, and steric stabilisation, resulting from the repulsive force arising when configurational entropy is reduced as particles come close to each other[1].

3.3.1 Zeta potential

The surface charge of a particle will affect its electrostatic stability and how it interacts with other charged species. Due to bound counter ions it is hard to directly measure the surface charge of particles, but it can be assessed in terms of the zeta potential (ζ), obtained here by measurements of electrophoretic mobility. It is called zeta potential simply because it is denoted by the Greek letter ζ. A higher absolute value of the ζ-potential indicates a higher stability[121].

Charged particles in a solvent will be surrounded by an electric double layer[1]. The inner so called Stern layer consists of tightly bound counter ions, and the outer diffuse layer is made up of less firmly associated ions (Figure 3.5). When the particle moves, ions within the diffuse layer up to the so called slipping plane, will move with it. The ζ-potential is defined as the potential at the slipping plane (Figure 3.5).

The electrophoretic mobility $U_E = v/E$ was here measured using laser Doppler electrophoresis. The velocity (v) of charged particles moving due to an applied electric field (E), is determined from intensity fluctuations of scattered light. The frequency of the intensity fluctuations will be equivalent to the Doppler shift due to particle motion between the incoming and scattered light. The ζ-potential is then related to U_E through the Henry equation

$$U_E = f(\kappa\alpha)\frac{2\epsilon\epsilon_0\zeta}{3\eta} \tag{3.10}$$

where ϵ is the dielectric constant of the medium, ϵ_0 is the permittivity of vacuum and η is the viscosity of the solvent. $f(\kappa\alpha)$ in Eq. 3.10 is the Henry function, where α is the effective radius of the particle and κ^{-1} is the Debye screening length, which can

be thought of as the "thickness" of the electric double layer. For particles much larger than the electric double layer, $f(\kappa\alpha)$ is equal to 1.5 according to the Smoluchowski approximation[1], which was used in this work. As the ζ-potential, like $\langle R_H \rangle$, was calculated from light scattering experiments, it will be strongly biased towards the charge of the largest particles.

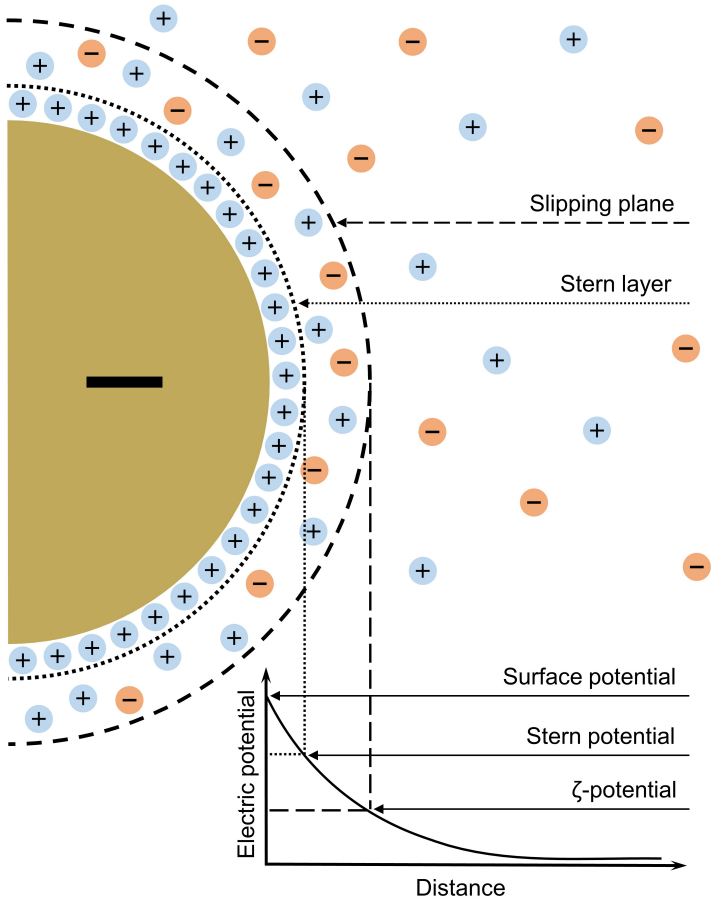

Figure 3.5 Schematic illustration of a charged particle with its electric double layer.

4 Characterisation of Dissolved Organic Matter

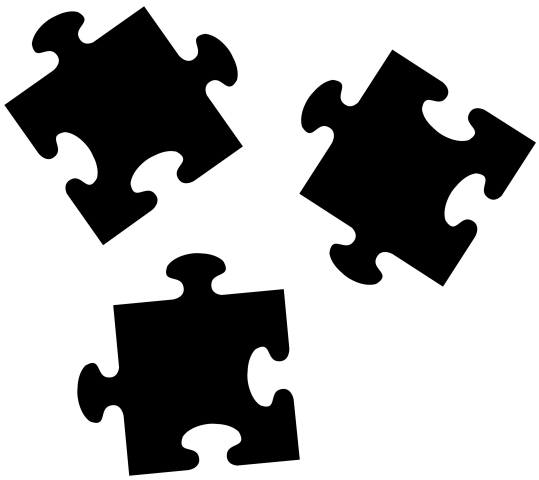

In this chapter, we present the main findings from Papers I and II, on the characterisation of DOM from the molecular to colloidal length scale, using our multi-method approach. We begin by looking at the chemical composition of DOM (Section 4.1), to lay out the boarders of our puzzle, and then we move on to the colloidal size and structure (Sections 4.2 and 4.3). Having established a basic understanding of these characteristics, we also touch upon the stability of colloidal DOM (Section 4.4), to add some more pieces to the overall picture. Most of the conclusions described here were made possible by investigating the variations of DOM, when changing the extraction protocol. In other words, we have studied how dissolution from soil is affected by physico-chemical factors. Indirectly, this may also tell us something about the properties of the original soil.

As mentioned in the introduction, there is not one clear definition of DOM. In order not to get lost in acronyms, DOM will throughout the rest of this thesis refer to the organic material extracted from soil by water or an aqueous solution, which is not retained upon filtration using a 200 nm pore size. With this upper size cut-off we obtain samples with minimal contamination of microbes, which can be stored and analysed for longer periods of time. This is also a suitable size range accessible with our scattering techniques. Although this is an operational definition of DOM phrased to be practical in laboratory studies, it has been shown that ca. 70% of particles in the mobile fraction of soil has a size < 200 nm[91], and would thereby be captured by this definition.

4.1 Chemical characterisation

To find our corner pieces, let us begin by investigating the chemical composition of the low molecular weight fraction of DOM, which was studied using solution ^{1}H NMR. As can be seen from the "forest" of peaks in Figure 4.1, DOM is a complex multicomponent system. We have been able to identify the specific peaks of a few individual compounds such as acetic acid (1.9 ppm, singlet), formic acid (8.3 ppm, singlet), ammonium (7 ppm, triplet), and what we believe to be ethanol (1.1 ppm, triplet and 3.6 ppm, quartet)[108,122,123]. The exact position of the acids vary with pH, and the ammonium triplet is only visible at low concentrations of NH_3, meaning at low pH.

To characterise the ^{1}H NMR spectrum, we divide it into regions (R) representing different compound classes as indicated in Figure 4.1. These are defined as R1 (0.6–1.65 ppm), "aliphatics" (–CH_2–); R2 (1.65–2.2 ppm), "acids" (–CH_2–COO–); R3 (2.2–3 ppm), "esters" (–CH_2–COO–R); R4 (3.0–4.3 ppm) "carbohydrates", and R5 (6.0–9.0 ppm), "aromatics"[122,124]. The water suppression technique used remove

the signal around 4.3–5 ppm, and the area of 5.0–6.0 ppm, which show resonances from alkenes, was excluded from analysis due to residual noise from the suppression. Note that the subdivision described here is a generalisation. For example, we see that formic acid and ammonium falls into the region of aromatics. It is also important to keep in mind that mainly small molecules having fast rotational dynamics will be detected, and that what we track is the signal from protons. This means that the sensitivity to substances containing few H will be low. Also, chemical groups where the protons have fast exchange with water, such as hydroxyl and carboxyl groups, will not be visible. For more details on the analysis of the ^{1}H NMR spectra, see also the discussion in section S1.4 in the Supplementary Material of Paper I.

Now that we have established how to read the ^{1}H NMR spectrum of DOM, we can continue with some observations. First, we see that the dominating component is carbohydrates (R4). It appears as if both low molecular weight carbohydrates and some larger molecules are present, respectively giving rise to the sharp peaks and a broader single resonance at the base. A clear signal from aliphatic components is also present, while almost no sharp signals from aromatics. The relative intensity of the different regions, which is proportional to the proton concentration, can be assessed by dividing the integral of one region, with the sum of integrals from all regions (hereafter referred to as total NMR intensity). As shown in the inset of Figure 4.1, this highlights the dominance of carbohydrates.

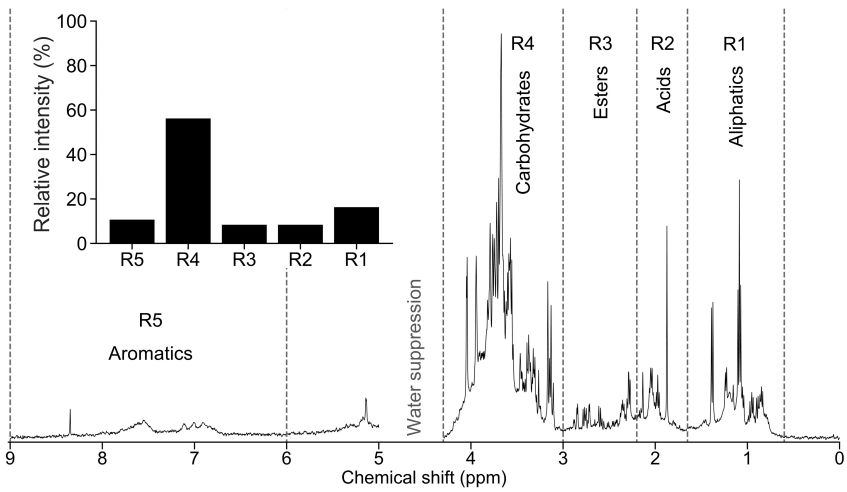

Figure 4.1 ^{1}H NMR spectra of DOM extracted at 4°C for 24h. Dashed lines mark the regions of different compound classes. The inset shows the relative concentration of different compounds, based on NMR intensity of the region.

As an additional chemical characterisation, solid state ^{13}C NMR was used in Paper I, on freeze dried DOM samples. Also here, the spectra can be divided into regions

representing different compound classes as shown in Figure 4.2. Similar to what was observed for the low molecular weight fraction by ^{1}H NMR, carbohydrates appear to dominate also the bulk signal. Resonances from aliphatic components and some carboxyls are also present. The aromatic signal is low, which could partially be due to long relaxation times of aromatic carbon. However, considering the hydrophobicity of aromatics, finding low concentrations in a water extract is not surprising. IR spectroscopy gave similar results as the NMR, indicating the presence of carbohydrates and aliphatic components, some signs of aromatics and also clay minerals which would not be detected with the other techniques. We can not estimate how much of these components that are present, as the IR signal is not quantitative. For more details on the IR and ^{13}C NMR analysis, see Paper I and sections S1.2 and S1.3 of the accompanying Supplementary Material.

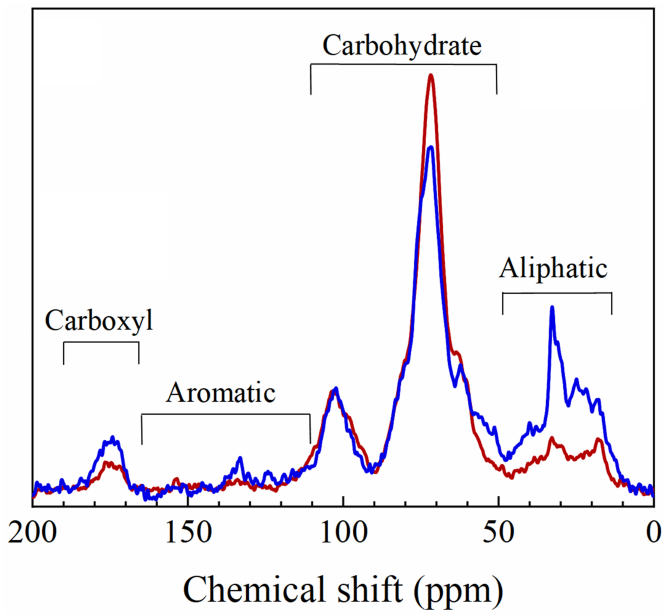

Figure 4.2 ^{13}C NMR spectra obtained using CP-MAS of freeze dried DOM, extracted at room temperature for 24h (blue) or 100°C for 1h (red). Regions of different compound classes are indicated. Modified figure taken from Paper I.

4.1.1 Effects of extraction protocol

The general results presented above apply to all water extracts investigated. However, varying extraction protocols have been used in the literature to obtain DOM, as described in the introduction, and previously also carefully assessed in terms of chemical differences[90,94,95,97]. To later interpret the information about the colloidal fraction, it

was however necessary to also asses with our techniques how the extraction procedure affected extracted amounts and chemical composition in our extracts. Considerable variations were indeed observed when changing the extraction procedure, and these observations were used to better understand the dissolution process of DOM from soil.

4.1.1.1 Effects of mechanical agitation

Mechanical agitation during extraction has a profound effect on the amount of DOM extracted. This can be seen in Figure 4.3 where we compare ^{1}H NMR spectra from extracts obtained at 4°C with and without the use of stirring during the extraction procedure. The total NMR integral was ca. 7 times higher with stirring compared to without. A similar relative difference was also observed in the TOC concentration. In Figure 4.3 we also see that the stirred extract contains relatively more narrow signals compared to the unstirred, showing the presence of small rapidly tumbling molecules. The fraction of carbohydrates also increased considerably, from ca. 30% to ca. 70% when using stirring. Increasing the extraction time from 24h to 7 days, omitting stirring, did increase the extracted concentration and number of narrow peaks, but not nearly as much as with stirring (Figure 4.3). This suggests a slow but continuous dissolution of DOM.

These observations are consistent with the view that stirring partially fragmented otherwise stable soil aggregates[72,74,96], exposing new surfaces to the water phase, and that a large part of the extracted DOM originated from these previously inaccessible sites. This view explains the observation of low molecular weight carbohydrates in the ^{1}H NMR spectra which may seem surprising, considering that microbes in soil are believed to be carbon limited[125,126]. Soil aggregates[74,75] thus act as a protected reservoir of such substances as only the surface material is exposed to microbes, while the interior is inaccessible due to very narrow pores as well as lack of water and low oxygen diffusion[77,78].

For all extractions described hereafter, stirring was used to obtain sufficient concentrations for analysis (within reasonable extraction time). This means we asses the soil material with the potential of becoming DOM, if exposed to the water phase.

4.1.1.2 Effects of extraction time and temperature

Extraction parameters often varied in literature are extraction temperature and time, with the extremes being room temperature or below (referred to as cold extraction), and boiling (100°C, referred to as hot extraction)[30,85,93]. In Paper I, we assessed dif-

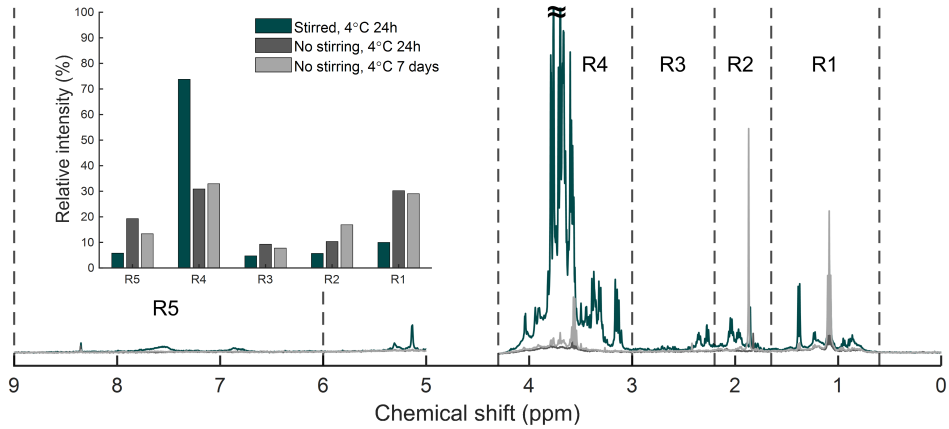

Figure 4.3 ^{1}H NMR spectra of DOM extracted at 4°C with stirring for 24h, and without stirring for 24h and 7 days. Dashed lines mark the regions for different compound classes. The inset shows the relative NMR intensity of the different regions. Modified figure taken from Paper II.

ferences between extracting at room temperature for 24h and boiling for 1h. In Paper II, we increased the data resolution by assessing extracts from 5 different temperatures between 4°C and 100°C, and three different extraction times at each temperature.

Increased extraction temperature greatly increased the concentration of TOC. The effect was most pronounced at temperatures above 50°C, where an effect of extraction time was also visible (Figure 4.4). The extraction behaviour of common nutrients (N, P, Fe) followed a similar trend (Figure 4.4). An interesting observation is that in the room temperature extracts, all concentrations were lower, likely due to microbial decomposition during extraction. This is supported by few narrow peaks observed in R4 in the ^{1}H NMR spectrum (Paper II, Figure 5), indicating that low molecular weight carbohydrates were decomposed. At 4°C, and temperatures above ca. 30°C, microbial activity is substantially decreased[50,51].

The total ^{1}H NMR intensity increased linearly with TOC for the different time and temperature extracts (Paper II, Figure S4). The overall composition remained similar, however, increasing extraction temperature increased the relative intensity from carbohydrates, while the intensity of aliphatics was higher at lower temperatures (Figure 4.5). This was also visible in the ^{13}C NMR (Figure 4.2). The pH decreased with increasing extraction temperature, from almost 6 in the cold extracts down to ca. 3 in the hot extracts, partially due to extraction of more small organic acids and possibly oxidation of sugars.

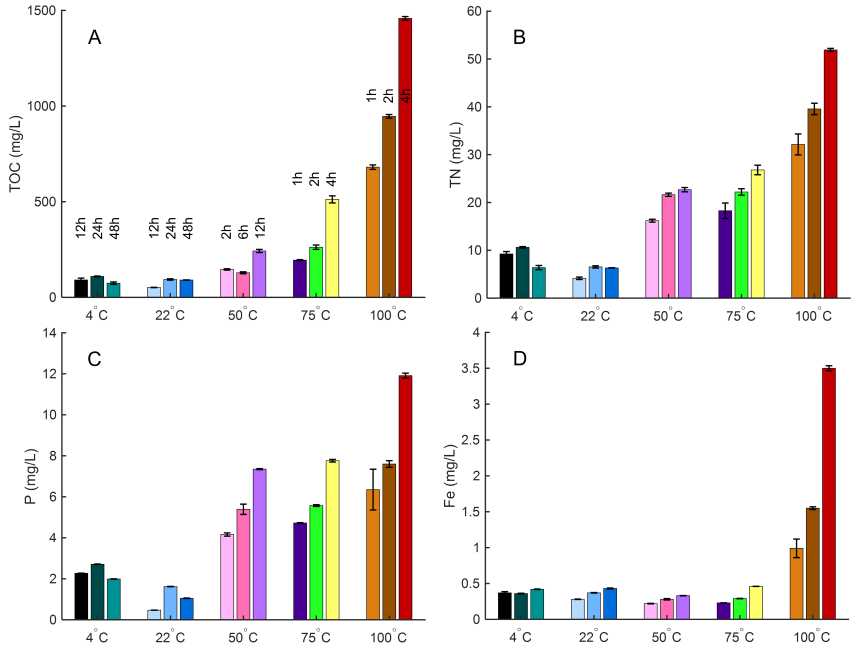

Figure 4.4 Elemental analysis of DOM extracts. Concentrations of A) TOC, B) TN, C) P and D) Fe in mg/L for all extraction temperatures and times assessed in Paper II. Times indicated in A) applies to the whole figure. Error bars represent one standard deviation based on measured triplicates from the same extract. Figure taken from SI of Paper II.

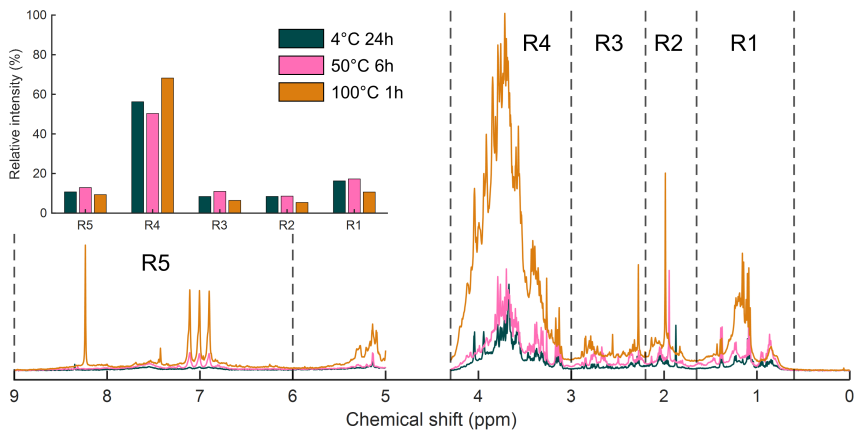

Figure 4.5 ^{1}H NMR spectra of DOM extracted at 4°C 24h, 50°6h and 100°1h. Dashed lines mark the regions for different compound classes. The inset shows the relative NMR intensity of the different regions. Figure taken from Paper II.

4.1.1.3 Effects of high pH

As mentioned in the introduction, alkaline extraction of SOM has been widely used and is known to give a high extraction yield. As the high pH will lead to deprotonation of many functional groups, we wanted to asses how this affect the dissolution of DOM.

Extraction at high pH had a similar effect on concentration as increased extraction temperature. We extracted DOM at 22°C for 24h using 0.1 M NaOH (pH 13), subsequently lowering the pH to 5.8 ($NaOH_{pH5.8}$) or 1.2 ($NaOH_{pH1.2}$) respectively, before filtration. The TOC of $NaOH_{pH5.8}$ was similar to the extract boiled for two hours and lowering the pH to 1.2 roughly decreased the TOC by half, compared to $NaOH_{pH5.8}$. This will be further discussed in Section 4.4. These extracts also contained high concentrations of TN, P and Fe (see Paper II). Despite the high TOC, the relative intensity of the ^{1}H NMR regions (Figure 4.6) was similar to that of a room temperature water extract. This means a relatively low fraction of carbohydrates and clear signals of aromatic and aliphatic components.

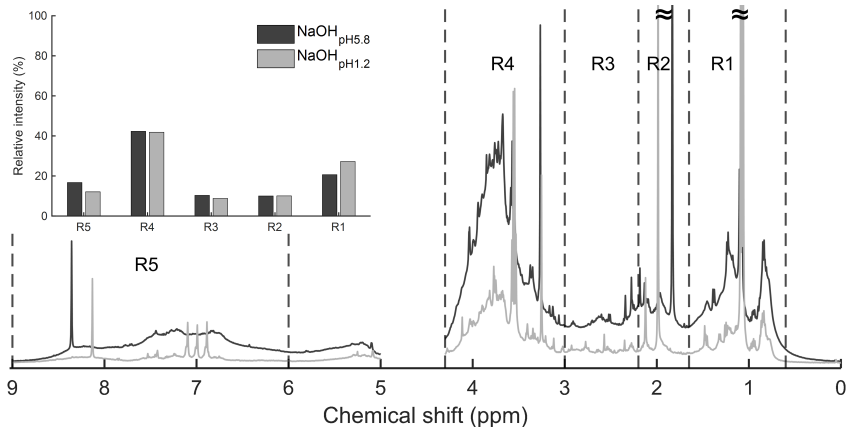

Figure 4.6 ^{1}H NMR spectra of DOM extracted at 22°C 24h using NaOH, pH adjusted to 5.8 or 1.2 respectively. Dashed lines mark the regions for different compound classes. The inset shows the relative NMR intensity of the different regions. Peaks marked with ≈ are cut in hight.

4.1.2 Monosugar composition

All spectroscopy techniques highlighted the dominance of carbohydrates. To learn more about these carbohydrates, an analysis of the monosugar composition was performed. Analysis of the original extracts reported on neutral sugars present in monomeric form, while polymeric sugar was analysed after acid hydrolysis (see details in the methods section of Paper I). The 7 different monosugars detected, and their relative

abundance, are reported in Table 4.1. Sugars in monomeric form were only detected when extracting at elevated temperature. This could however be an effect of microbial activity during the extraction at ambient temperature, as discussed above.

Table 4.1 Relative abundance of different neutral sugars (monomeric+polymeric) detected in DOM extracted at 22°C for 48h and 100°C for 1h. Monomeric sugars constituted 15% of the total sugar concentration in the 100°C extract, while non were detected in the 22°C extract.

Sample	Fucose	Galactose	Glucose	Xylose	Mannose	Rhamnose	Arabinose	Total concentration
22°C 48h	5.6%	23.3%	23.3%	9.1%	17.2%	13.2%	8.3%	98.7 mg/l
100°C 1h	3.6%	26.4%	33.8%	6.7%	10.8%	18.7%*		857.0 mg/l

*Rhamnose and arabinose were not separated in the analysis of the 100°C sample. The calculation of the combined concentration was based on arabinose.

Let us take a moment to speculate on the origin of the different components observed. The monosugar composition tells us that the observed carbohydrates are primarily not cellulose, which only consists of glucose units. This agrees with the low solubility of cellulose in water, however some partially degraded cellulose fibrils could pass the filtration step. If the carbohydrates are of plant origin, an option could be hemicellulose which may have a higher water solubility. This option is supported by the presence of mannose, and especially xylose and arabinose, two monosugars which are seldom produced by microbes[127]. The soil originates from a spruce forest and could contain a lot of the hemicellulose galactoglucomannan, which is one of the main components of the secondary plant cell wall of conifers[128,129], and also xyloglucan found in the primary cell wall[130]. However, a large fraction of the carbohydrates may be of microbial origin. Soil bacteria contains a lot of glucose, ribose, galactose and rhamnose, while they secrete extracellular polymeric substances (EPS) containing mainly mannose[127]. It should however be noted that no ribose was detected in the DOM samples. It is not possible to deduce the exact origin of the different carbohydrates, they are likely a mix of hemicelluloses and some microbially derived components.

The aliphatic components observed could be lipids or different waxes. Waxes which contain a variety of different fatty acids, fatty alcohols and alkanes are abundant on the surface of conifer needles[131,132].

Two main questions are raised by the results of the chemical analysis: why do we extract more DOM at higher temperature and pH, and why do we get a higher fraction of carbohydrates at higher temperature? To be able to answer these questions and relate them to the dissolution process of DOM, information on the effects of extraction on the colloidal structure is also needed.

4.2 The structure of colloidal DOM

Roughly half of the DOM can be accounted to the colloidal fraction, as assessed by the change in TOC after dialysis experiments (Paper I). A similar observation was made from assessments of microbial decomposition (Chapter 5 and Paper III). The dialysis pointed to a lower fraction of colloidal material in hot extracts (around 40%), while a higher fraction of colloidal material was observed for room temperature extracts (50–70%). However, as microbial mineralisation during extraction (see previous discussion) was not considered in this comparison, the result is likely skewed by initial removal of some low molecular weight substances in the room temperature extracts. Dialysed samples were still dominate by carbohydrates.

The overall size of the largest DOM colloids was assessed by the z-averaged hydrodynamic radius, $\langle R_H \rangle$, obtained from DLS. In agreement with the filter cut-off size of 200 nm used, an $\langle R_H \rangle$ of around 100 nm was generally observed, with a PDI around 0.3 indicating a rather wide polydispersity. The exception was extracts obtained at 100°C, and partially 75°C, where $\langle R_H \rangle$ of up to 130 nm were observed and the PDI was around 0.5. The reason for this will be discussed in Section 4.4. The colloidal structure was further investigated using static scattering, mainly SAXS but also in combination with SLS to access the complete size range of the colloidal DOM. We return to our different extraction procedures to track the effects on colloidal structure.

4.2.1 Effects of mechanical agitation

The colloids extracted with and without stirring had a similar structure. In figure 4.7 we observe the same shape of the SAXS patterns, highlighted also by the approximately constant value of the ratio between the intensities at all q, shown in the inset. The intensity is about a factor of 8 higher for the extract with stirring, in rough agreement with the difference in concentration based on TOC. The longer extraction time of 7 days did not result in a higher scattering intensity, suggesting that the available colloids were already released early during the extraction. Taken together, these results indicate that colloids with a similar structure are present both as an easily extractable mobile phase in the soil, and in occluded form inside soil aggregates.

The scattered intensity followed a power law decay $I(q) \propto q^{-D}$ over roughly the full q-range observed, with $D \approx 2.8$ (Figure 4.7). Here, D represents a fractal dimension and $D \leq 3$ indicates a mass fractal, describing how the mass of the system scales with the linear dimension[112,133]. For a homogeneous object with a smooth surface only having one characteristic dimension, e.g. a sphere, $D = 4$[112].

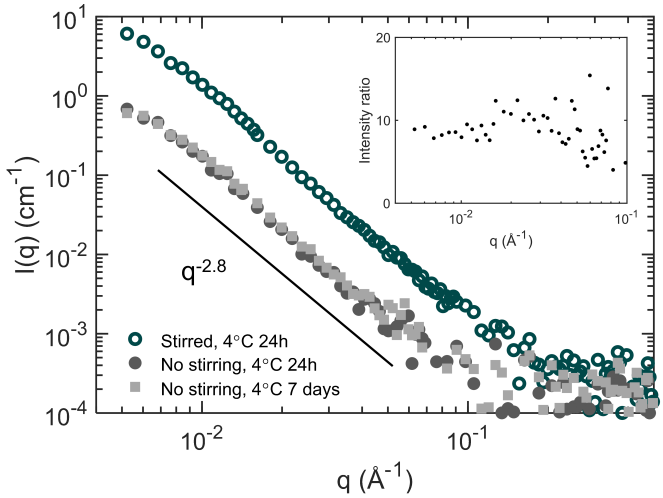

Figure 4.7 SAXS pattern of DOM extracted at 4°C with stirring for 24h, and without stirring for 24h and 7 days. The black line represents a slope of $q^{-2.8}$. The inset show the intensity ratio between DOM extracted for 24h with and without stirring. Modified figure taken from Paper II.

4.2.2 Effects of extraction temperature and time

Extraction temperature and time did have a significant effect on the colloidal structure. As shown in Figure 4.8, the scattered intensity at low q (< 0.03 Å^{-1}), probing large structures, decreased with increasing extraction temperature. The opposite trend was observed at high q-values, most pronounced for 100°C extracts. This suggests a gradual shift in the concentrations of large and small colloids with increasing extraction temperature, becoming more pronounced with longer extraction time. Both the intensity decrease and increase was about one order of magnitude. However, as large colloids result in higher scattering intensity, a higher concentration of the smaller size fraction would be needed to result in the same intensity difference, assuming a similar contrast factor.

To confirm that the change in the scattering pattern observed as a function of temperature was due to a change in concentration of two separate colloidal species, centrifugation was used. Figure 4.9 shows the scattering patterns of one cold and one hot DOM extract before and after centrifugation. As seen, the intensity at high q remains constant, while the intensity at low q decrease after centrifugation. This indicate that we can remove a fraction of the larger colloidal species and still retain the same concentration of the smaller size fraction. Thus, the scattering pattern report on the presence of two separate colloidal species of different size.

Model calculations were used to quantitatively analyse the static scattering data. The

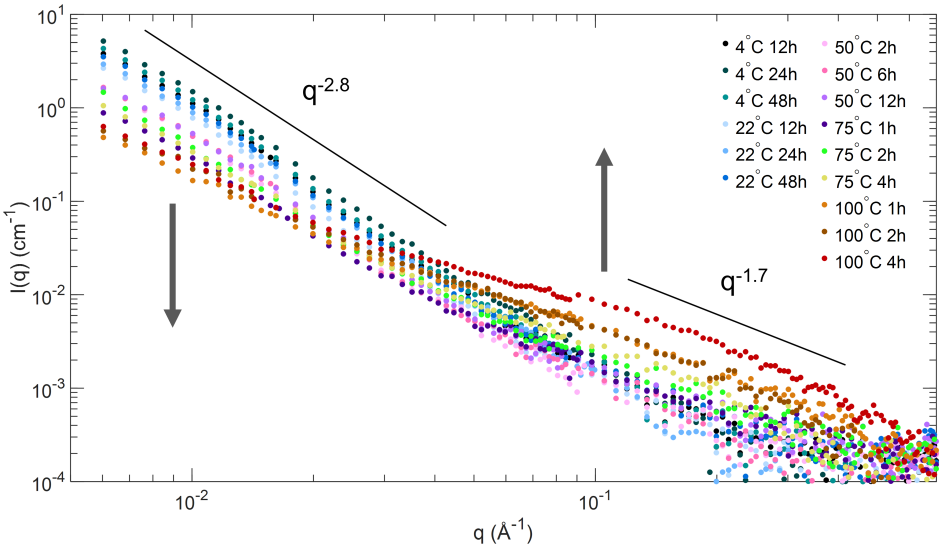

Figure 4.8 Scattering patterns of DOM extracted at all temperatures and times assessed in Paper II. Arrows indicate the general trends observed with increasing extraction temperature. The black lines represent slopes of $q^{-2.8}$ and $q^{-1.7}$ respectively.

model contains two species: mass fractal aggregates, here called clusters, and linear polymer chains, here called coils. The second species was chosen based on the chemical analysis, showing a large fraction of polymeric sugars increasing in concentration with temperature, similar to the scattering at high q. In the scattering patterns of hot extracts in Paper I, a region of $D \sim 1.7$ was also observed, indicative of scattering from polymers[112,134]. Because of the low concentrations, we neglected particle interactions and assumed $S(q) = 1$ in all calculations. A linear combination of the two contributions was used, according to $I(q) = I_{coil}(q) + I_{cluster}(q)$.

The scattered intensity of the respective species can be written as

$$I_x(q) = \frac{c_x M_x}{d_x^2 N_A} \Delta\rho_x^2 P_x(q) \tag{4.1}$$

where x denotes cluster or coil respectively. Here c_x is the concentration in mass per unit volume, M_x is the weight average molar mass, d_x is the mass density, N_A is Avagodro's number and $\Delta\rho_x$ is the SLD difference between solvent and scatterer. As the form factor for clusters, $P_{cluster}(q)$, we used the corrected Beaucage model[135], characterising the clusters by a radius of gyration, R_g, and a mass fractal dimension, D. The form factor used for $P_{coil}(q)$, describes semi-flexible cylinders with excluded volume interactions[136,137], giving chain conformations resembling a self-avoiding random walk. The semi-flexible cylinders are characterised by a contour length L, a cross section radius r, and a Kuhn length λ_k describing the local stiffness.

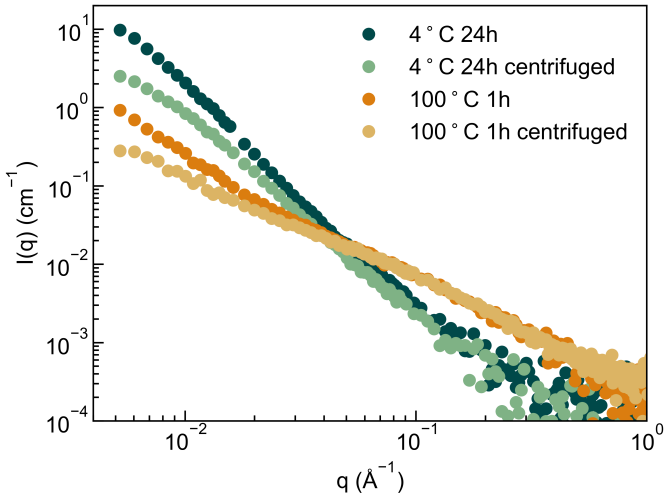

Figure 4.9 Scattering patterns of DOM extracted at 4°C for 24h and 100°C for 1h, compared with the supernatant after centrifugation at 20000g and 25000g, respectively.

A number of assumptions were required to put numbers on all of these parameters. The first assumption, was that both coils and clusters are composed of hemicellulose with an average chemical formula $(C_5O_4H_8)_n$ [138] and a density of 1.5 g/cm^3 [139]. This provides a value for $\Delta\rho_{coil} = \Delta\rho_{cluster} = 4 \times 10^{10}$cm^{-2}. The contour length (in Å) was calculated as $L = 5M_{coil}/M_{C_5O_4H_8}$, where 5 Å is the approximate effective length of an anhydroglucose unit [140]. Further assumptions were to fix $r = 3$ Å and $\lambda_k = 20$ Å, corresponding to approximately 4 glucose units. For the clusters, $R_g \approx 70$ nm was obtained from SLS data and D was determined from the slope of the low q-region of each scattering pattern. This leaves the concentrations and molecular weights of the coils and clusters respectively, as free parameters. As seen from Eq. 4.1, these appear as a product and can not be determined individually. However, by assuming a constant molecular weight for each species, we could obtain concentrations that could be used for relative comparisons between different extracts. In the different papers, $M_{coil} = 3 \times 10^3 - 1.5 \times 10^4$ g/mol and $M_{cluster} = 1 \times 10^8 - 1 \times 10^9$ g/mol have been used.

The combined SAXS and SLS data from DOM extracted at different temperatures was simulated using the described model, achieving good agreement (Figure 4.10). A contribution from $I_{coil}(q)$ was only used for DOM extracted above room temperature. With increasing extraction temperature, $c_{cluster}$ decreased, while the lower molecular weight assumed for the coils meant the concentration of this species had to increase considerably to match the scattered intensity (Table 4.2). D used was approximately constant (Table 4.2).

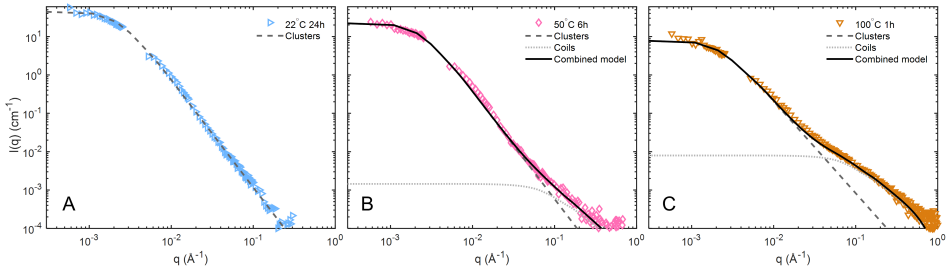

Figure 4.10 Scattering patterns of DOM extracted at A) 22°C 24h, B) 50°C 6h and 100°C 1h. Model calculations of $I_{cluster}(q)$, $I_{coil}(q)$ and the linear combination are shown. Parameters used are found in Table 4.2. Figure taken from Paper II.

Table 4.2 Model parameters used for the calculations shown in Figure 4.10. Here $M_{cluster} = 1 \times 10^9$ g/mol and $M_{coil} = 3 \times 10^3$ g/mol were used.

Sample	$c_{cluster}$ (mg/l)	c_{coil} (mg/l)	D
22°C 24h	40	0	2.8
50°C 6h	20	400	2.8
100°C 1h	7	2200	2.4

4.2.3 Effects of high pH

High pH extraction appeared to have a similar effect on the colloidal structure as high temperature. As seen in Figure 4.11, the SAXS patterns of $NaOH_{pH1.2}$ and $NaOH_{pH5.8}$ contains a contribution from the small sized colloids modelled as coils. $NaOH_{pH5.8}$ also appears to contain a high fraction of clusters and show the highest scattering intensity recorded for any of our extracts over the whole q-range, although the TOC was similar to that obtained from 2h boiling. The scattering pattern of $NaOH_{pH1.2}$ roughly overlaps with that obtained from 2h boiling despite having half the TOC concentration. These observations could indicate contributions to the scattering from other high contrast materials.

4.2.4 Contrast variation

A remaining question is the actual composition of the two different colloids. In our model we assume pure hemicellulose, but the chemical analysis show that also other types of organic molecules, as well as clay particles, Fe and P are present in the soil extracts. At low temperature, we only observe one colloidal species in the scattering pattern. One possibility is thus that this species, the clusters, is a composite material

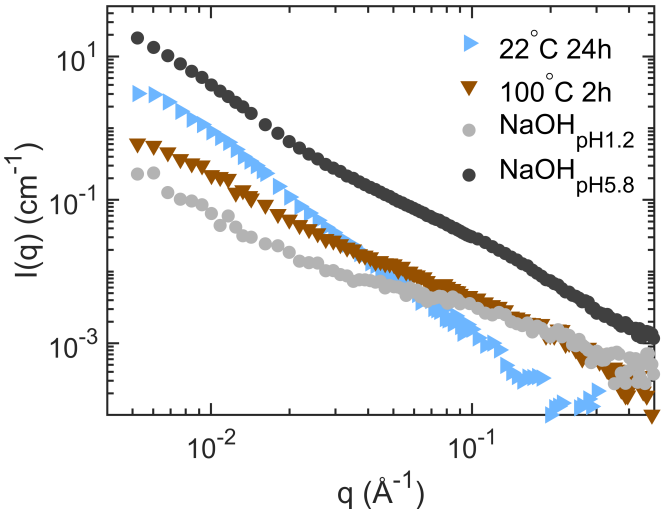

Figure 4.11 SAXS patterns of $NaOH_{pH1.2}$ and $NaOH_{pH5.8}$ compared with water extracts of 22°C 24h (the time and temperature used for NaOH extractions) and 100°C 2h (having a similar TOC as $NaOH_{pH5.8}$)

containing all the different chemical components identified. The clusters could for example be aggregates rich in carbohydrates, held together by some gluing agent such as EPS[48] or some waxes. The plant wax nonacosan-10-ol common in conifers, have been shown to have a melting point around 80°C[141], which is in agreement with the temperature where clear changes are visible in the scattering patterns of DOM (Figure 4.8). However, from our data we can not rule out that a low concentration of coils or other small particles of different chemical components are present also in low temperature extracts. The scattering contribution from such species could be covered by the stronger intensity from the larger clusters.

The colloidal composition was investigated using contrast variation SANS (Paper IV), as described in Section 3.2.1.2. For a pure compound, $I(q)$ is zero at the match point. For a composite particle however, $I(0) \rightarrow 0$ at the average match point, while contrast between internal components of different SLDs will result in a variation in the overall shape of the scattering pattern, at different contrast conditions[111,142].

A match point around 40% D_2O was estimated for DOM (Figure 4.12 A), in agreement with the overall match point of polysaccharides[115], and thereby in agreement with the main result from the chemical analysis. The SANS experiment was performed on freeze-dried DOM from hot extraction but based on the similarity in composition observed, we believe the result to be valid as an average SLD also for cold extracts. The change in intensity at low q as a function of D_2O volume fraction (ϕ_{D_2O}) followed the behaviour of a species with SLD $= 1.8 \times 10^{10}$ cm^{-2}, with two H exchangeable for D at

increasing ϕ_{D_2O} (Figure 4.12 A). This agrees with the chemical formula $(C_5O_4H_8)_n$ and a mass density of 1.5 g/cm^3, as also used in our previous model calculations. No change in the shape of the scattering patterns could be observed at the different contrast conditions. This suggests a similar composition of the two colloidal species, although the data was very noisy making any reliable determination difficult.

To specifically investigate the composition of the clusters, three different contrast conditions were compared for DOM extracted at room temperature: SANS in a solvent of ϕ_{D_2O}=0.3 (low contrast) or ϕ_{D_2O}=1 (high contrast), in comparison to SAXS. As observed in Figure 4.12 B, the shape of the scattering patterns were similar for all three different contrast conditions, and the shape also agreed with our previous model of mass-fractal clusters. This suggests that the clusters are essentially pure, one component colloids, likely composed of carbohydrates. Alternatively, the similarity in shape at different contrast conditions could also arise if the material was chemically mixed on a length scale smaller than what is resolved in our experiments. Meaning essentially on a molecular length scale.

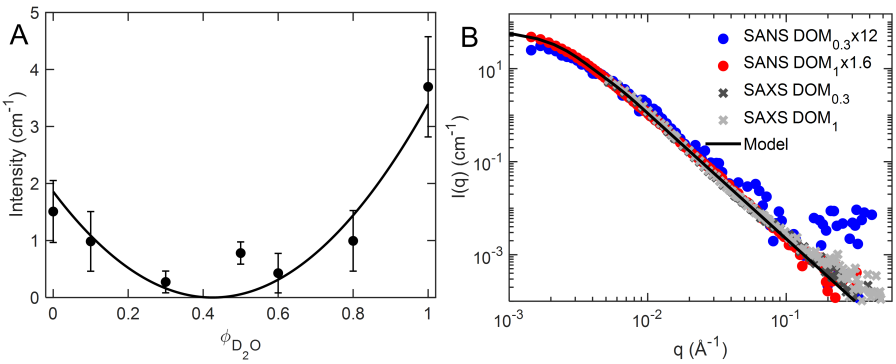

Figure 4.12 A) Variation in scattering intensity at low q (mean value of 10 first data points ± one standard deviation) for freeze-dried DOM redissolved in 7 different volume fractions of D_2O. The solid line represents a theoretical intensity variation for a species having an SLD of 1.8×10^{10} cm^{-2} with 2 exchangeable hydrogen. B) Scattering patterns measured by SANS and SAXS of DOM extracted at room temperature with ϕ_{D_2O}=0.3 or 1 respectively. The SANS data is scaled to the intensity of the SAXS patterns using a constant as noted in the legend. The solid line represents our model of clusters. Figure taken from Paper IV.

4.2.5 Conclusions

Our interpretation of the combined results, is that the clusters are aggregates of smaller components which have a low solubility in water, but are dispersed or fragmented by higher extraction temperature or high pH (Figure 4.13). The dispersion leads to a higher concentration of small components able to pass the 200 nm filter, and thereby to a higher concentration of DOM. Dilution series (Paper I) have shown that the

clusters are strongly associated, and do not disperse upon dilution. The strength of the aggregation was also evaluated by ultrasonication of cold extracts, and no difference was visible in the SAXS patterns before and after sonication.

The size fractionation observed could be a pure solubility effect, where the water solubility of carbohydrates, constituting the main component of the clusters, increase with temperature, and lead to dissolution into individual polymers. Hemicelluloses have previously been dissolved at temperatures similar to those where we observe changes in the scattering pattern[143,144], providing some support for this hypothesis. The fact that the colloidal structure of DOM is altered in a similar way by high pH as by high temperature could further support this hypothesis. Strong alkaline conditions have been used for over a century to dissolve or process cellulose[145]. The molecular mechanism behind the increased solubility involves the titration of the carbohydrate hydroxyl groups[116,146] which could have a similar effect on hemicellulose. Strong alkali is also known to dissolve lignin[147], which could be present and act as a possible gluing agent in the clusters or soil aggregates.

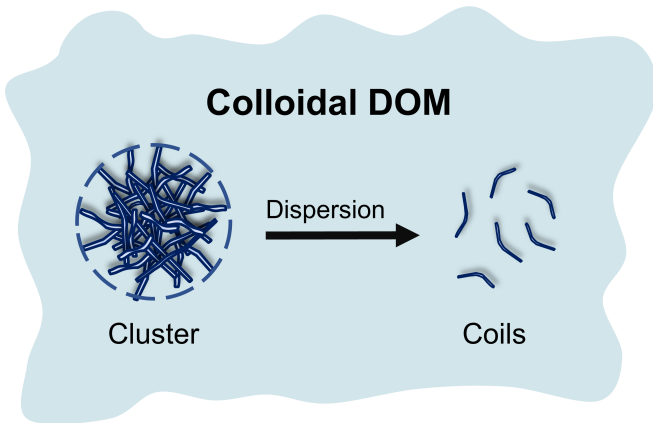

Figure 4.13 Schematic illustration of the colloidal structures observed in DOM, according to our model of the scattering data. Not drawn to scale.

4.3 The cryo-TEM Zoo of colloidal DOM

In addition to scattering methods, cryo-TEM was used to identify the colloidal structure of DOM. Several different structures were observed in cryo-TEM images of DOM extracted at room temperature. Figure 4.14 A-B show structures we believe to correspond to the clusters identified with scattering. These have low contrast, as expected for an organic material, a size around 200 nm and show indications of internal structure. Another, more rarely observed organic colloidal structure is shown in

Figure 4.14 C. These long stiff fibres of low contrast, where the stiffness indicate that this is a crystalline material, we assume to be fragments of cellulose fibrils. In addition, high contrast inorganic colloids were occasionally also observed. Figure 4.14 D show an example of high contrast particles which could for example be silicon or metal oxides. There is no visible indication of organic material associated with these particles. Finally, Figure 4.14 E show a high contrast particle identified as clay tactoids[148] and also here, there is no visible organic material in direct contact.

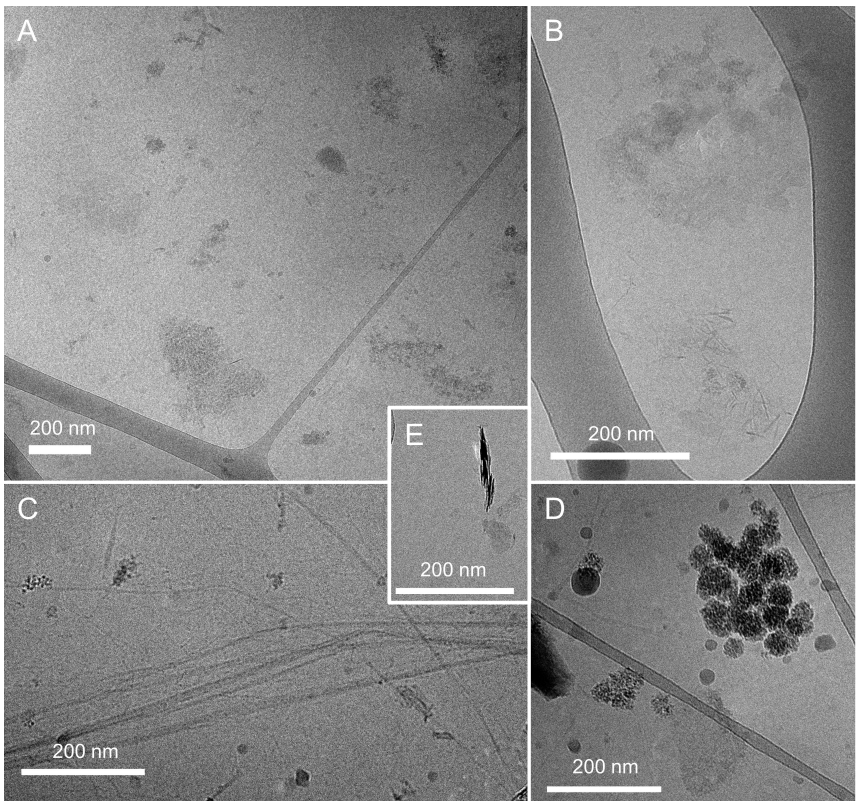

Figure 4.14 Cryo-TEM micrographs of different structures identified in DOM extracted at room temperature for 24h in 30% D_2O. A-B) Low contrast clusters, C) structures believed to be cellulose fibrils, D-E) high contrast particles. All scale bars represent 200 nm.

4.4 Stability of colloidal DOM

The colloidal DOM clusters are charge stabilised. All DOM extracts had a negative ζ-potential and presumably carboxyl groups, which generally have a pK_a around 4–5, determined the pH dependent charge of the colloids. The ζ-potential as a function

of extract pH is plotted in Figure 4.15 A for different temperature extracts, showing a linear decrease of the absolute value with decreasing pH. This indicate a decreased charge stabilisation at low pH. The larger $\langle R_H \rangle$ and PDI observed in extracts from 100°C and also 75°C mention in Section 4.2, thus indicate aggregation of colloids due to low electrostatic stabilisation. Aggregation, indicated by a quickly growing $\langle R_H \rangle$ and PDI, could also be induced in cold extracts by lowering the pH (pH $\approx$ 2, ζ-potential ≈ -5 mV).

Tracking the stability of a 100°C extract over time showed that it is mainly the largest colloids, the clusters, which aggregate. Figure 4.15 B show no change in the SAXS pattern after one month storage while the SLS data indicate aggregation of the larger colloids. When re-boiling the aged extract, the original shape was recovered and thus, the aggregated clusters appears to be re-dispersed by boiling. Over the time scale of months to years, sedimentation was observed in both hot and cold extracts. The higher electrostatic stabilisation at higher pH is thus not sufficient to keep the colloids stable for very long periods of time.

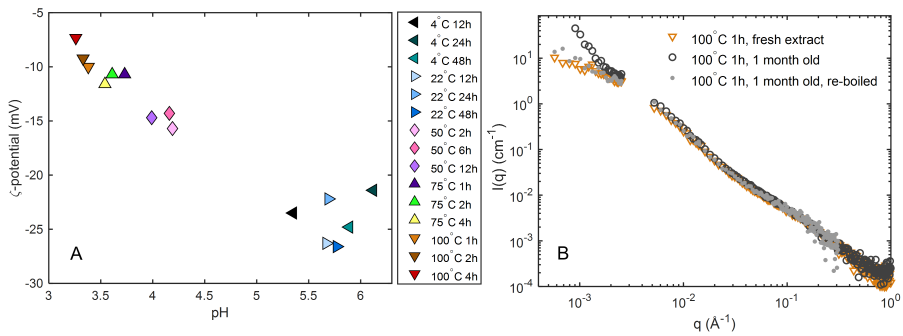

Figure 4.15 A) ζ-potential as a function of pH for DOM extracted at all temperatures and times assessed in Paper II. B) Scattering pattern of DOM extracted at 100°C for 1h, when measured within 12h from extraction (fresh), after one month storage, and after re-boiling the stored extract. The data from the re-boiled extract was scaled to the intensity of the previous, for comparison. Figure taken from Paper II.

The charge stabilisation can also be assessed from the pH adjusted NaOH extracts. Lowering the pH from 5.8 to 1.2 (ζ-potential ≈ -1.4 mV) resulted in an almost two orders of magnitude decrease in intensity at low q and one order of magnitude decrease at high q (Figure 4.11). This agrees with the clusters being charge stabilised and the low pH likely leading to aggregation, and removal of clusters from solution during filtration. The strong signal of coils remaining, suggests that this species is not dependent on charge stabilisation to remain in solution. It is still unclear what leads to the colloidal stability of the smaller species, but it could remain in solution simply because of a higher water solubility.

5 Bacterial decomposition of Dissolved Organic Matter

"If we knew what it was we were doing, it would not be called research, would it?"
– Albert Einstein

In this chapter we describe bacterial decomposition of DOM, based on the findings presented in Paper III. We make use of our detailed chemical and structural characterisation of DOM presented in the previous chapter, allowing us to compare the bioavailability of different DOM fractions.

One of the main reasons for the interest in DOM is, as discussed in the introduction, that this fraction of soil is considered mobile and bioavailable. We have however seen that DOM is composed of both a low molecular weight fraction and a colloidal fraction, both of which appear rich in carbohydrates. Does the bioavailability of these two fractions differ? Do colloidal size and structure affect the susceptibility of DOM to decomposition?

5.1 The experiment

There are many different types of decomposers present in soil, of which bacteria and fungi are the main litter decomposers[23]. In this study we have focused on bacterial decomposition, as this can be performed directly in the DOM extracts. An inoculum was obtained by shaking the same soil as used for the DOM extractions with water, and filtering the mixture down to a size of 1.6 µm. The size cut of used was the only restriction on what kind of microbes that were actually present in the inoculum. This means that apart from bacteria, it may include archaea, viruses and possibly some predators (bacterivorous protists)[149].

The inoculum was added to DOM extracted at 4°C for 24h (here referred to as cold) and 100°C for 1h (here referred to as hot) respectively, to be able to compare the bioavailability of our two different identified colloidal species (clusters and coils). The samples were incubated in the dark at room temperature for 2 months, being aerated and gently shaken approximately every second day. The concentration of TOC was initially ca. 10 times higher in the hot extract (≈1150 mg/l) than in the cold (≈100 mg/l) and the pH was ca. 3 unites lower, in accordance with the results presented in Chapter 4. To increase the electrostatic stability of the colloids and have comparable conditions, the pH of the hot extract was adjusted to the original pH of the cold extract (pH=5.9) before inoculation.

5.2 Decomposition kinetics

The extent of decomposition was quantified by the change in TOC concentration. As shown in Figure 5.1, TOC decreased by approximately 50% during the two months incubation, in both the cold and the hot extract. In the cold extract, the decrease was

fast during the first two weeks, after which it remained constant for the rest of the incubation period. In the hot extract, a more gradual decrease of TOC was observed and the concentration did not reach a constant value within the two months. These observations suggest that the bioavailable carbon was mineralised in the cold extract, while there could still be available carbon remaining in the hot extract.

The ^{1}H NMR spectra of the cold extract showed a removal of all sharp peaks within one week (Figure 5.2). This indicate that all low molecular weight substances detected by NMR were decomposed. The spectra of the hot extract decayed slower and some sharp features remained, in agreement with the idea that available material could still be present. No new peaks indicative of degradation products were observed in either of the extracts. Low molecular weight substances belonging to all kinds of compound classes identified were mineralised. This can be assessed by subtracting the spectra of the last time point from the initial spectra, as shown in the insets of Figure 5.2, representing the removed signal.

The degree of mineralisation of the low molecular weight fraction specifically, was assessed by the change in total NMR intensity (NMR_{int}) over time. Also this quantity decreased by roughly 50% during the incubation, slightly more in the hot extract than in the cold (Figure 5.1). A similar decay behaviour as for TOC was observed for NMR_{int}, in the cold and hot extracts respectively.

DOM mineralisation is often analysed in terms of an exponential decrease of TOC, or a sum of exponentials, each characterised by a decay rate or a decay time[40,150,151]. Here, we have used a similar approach and quantified the decomposition kinetics according to

$$\frac{A(t)}{A_0} = f_l e^{-k_l t} + (1 - f_l) \tag{5.1}$$

where $A(t)$ represents TOC concentration or NMR_{int} at time t and A_0 is the value at $t = 0$. f_l describes the labile fraction of DOM, $(1-f_l)$ is a stable fraction that does not decompose within the two months observation time and k_l is a rate constant. Observe that this is a simplified description as the components of DOM are more likely to behave according to a continuum of reactivity[152]. Eq. 5.1 has been fitted to the data in Figure 5.1 and the parameters are given in Table 5.1. To better determine the k value for NMR_{int} of the cold extract, where the initial decay phase was not captured, complementary measurements were performed during one week on a separate cold extract referred to as $Cold_s$.

Table 5.1 Labile fraction (f_l) and decay rate (k_l) with 95% confidence bounds, obtained from Eq. 5.1, when fitting the decrease in TOC concentration and total NMR intensity (NMR_{int}) over time, for the cold and hot extracts respectively.

	Cold		Hot	
	TOC	NMR_{int}	TOC	NMR_{int}
f_l (%)	50 ± 6	56 ± 4	52 ± 7	86 ± 9
k_l (day^{-1})	0.155 ± 0.076	0.303 ± 0.099	0.037 ± 0.009	0.022 ± 0.003

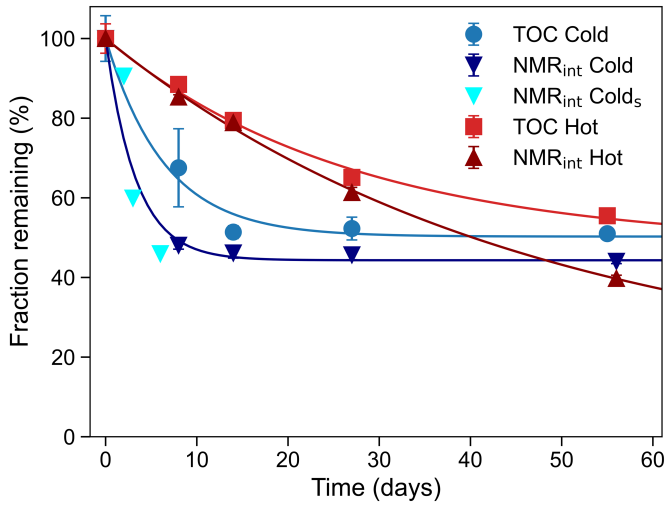

Figure 5.1 Remaining fraction of TOC and total NMR intensity (NMR_{int}) expressed as %, as a function of incubation time. Symbols represent mean values $\pm$ one standard deviation from triplicates. The data from $Cold_s$ was not replicated. Lines are fits according to Eq. 5.1, with parameters given in Table 5.1. Figure taken from Paper III.

The striking similarity in decomposition behaviour tracked by the TOC and NMR suggests that low molecular weight substances dominated the labile fraction. For the cold extract, both TOC and NMR_{int} gave a labile fraction of ca. 50%, however NMR indicated a faster decay rate. The small discrepancies observed could be due to different H/C ratios of remaining substances, meaning signal response will vary if tracking C (TOC) or H (^{1}H NMR). For the hot extract, NMR_{int} gave a clearly higher labile fraction (86%) than TOC (52%). However, these values are highly uncertain as the data had not yet reached a plateau. The initial overlap suggests that low molecular weight substances dominated the labile fraction also in the hot extract, during at least the first month of decomposition. A continued decomposition of small highly H-containing molecules, contributing to a larger degree to the NMR signal than to the total carbon content, could explain the discrepancy at later time points. The ca. ten times lower rate constant obtained for the hot extract is likely an effect of

oxygen deficiency. Considering the solubility of oxygen in water (ca. 10 mg/l at 20°C) and the high concentrations of carbon decomposed, it is possible that the bacteria experienced anaerobic conditions between aerating occasions. Anaerobic conditions may slow down the decomposition[49], and this effect would be more pronounced in the hot extract than in the cold, due to the initially higher TOC, with similar concentrations of accessible oxygen.

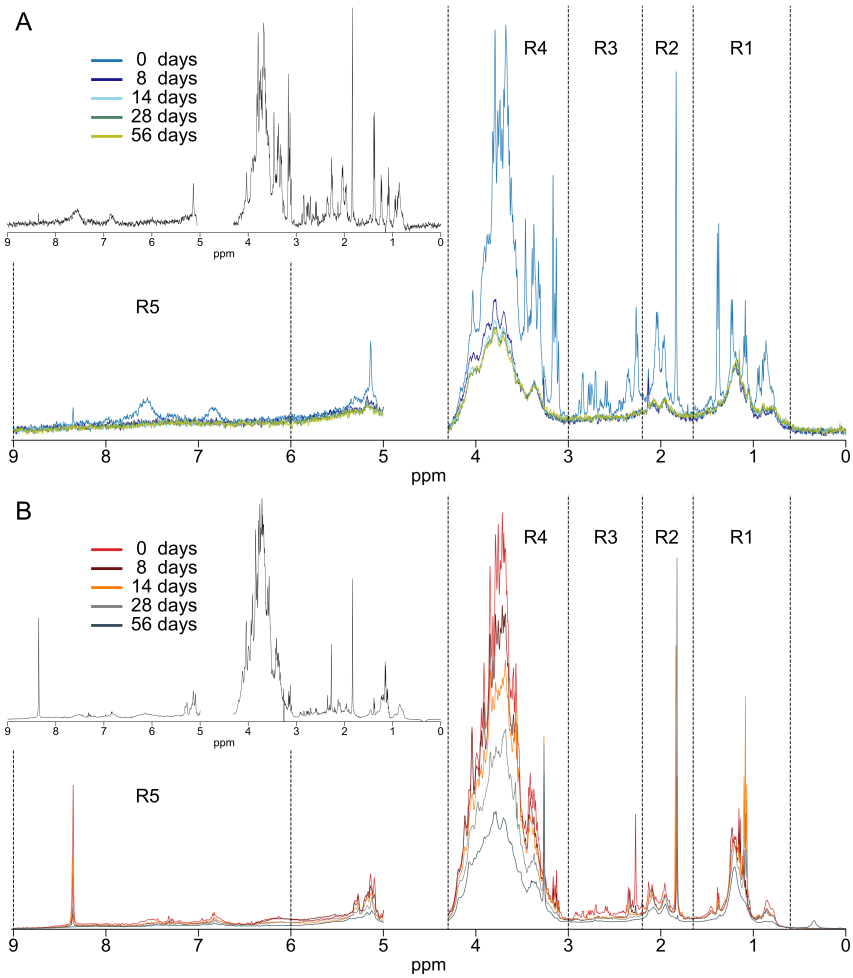

Figure 5.2 ^{1}H NMR spectra of A) cold and B) hot DOM extracts measured over time, during the two months incubation. Dashed lines represent the regions of different compound classes described in Section 4.1. The insets show the difference between the spectra of the first and last time points, representing decomposed material. Figure taken from Paper III.

In order to discuss the functional form of the decay, we may consider some different simple models or scenarios for the decomposition of a substrate, S, by bacteria, B. An exponential decay of the concentration $[S]$ implies that the rate $d[S]/dt \sim [S]$, i.e. is

proportional to the concentration $[S]$. In the case that S is decomposed in a simple binary "reaction"

$$S + B \rightarrow \textit{decomposition} \tag{5.2}$$

we can write

$$\frac{d[S]}{dt} = -k[B][S] \tag{5.3}$$

where k is a rate constant. Integration of Eq. 5.3 gives

$$[S] = [S]_0 \, e^{-k[B]t} \tag{5.4}$$

where $[S]_0$ is the initial concentration at t =0. For the case of respiration, O_2 should also be considered in the reaction scheme (Eq. 5.2). For this discussion, however, we for simplicity assume a steady state oxygen concentration, or similarly a large excess, so that this constant concentration can be incorporated into k.

Another model could be that the rate determining step for the decomposition is a slow machinery in the bacteria, which can than only decompose a limited number of substrate molecules per unit time. In this case, the rate is not proportional to $[S]$, but only to $[B]$ and we have instead of Eq. 5.3

$$\frac{d[S]}{dt} = -k[B] \tag{5.5}$$

with the solution

$$[S] = [S]_0 - k[B]t \tag{5.6}$$

which can also be written

$$\frac{[S]}{[S]_0} = 1 - \frac{k[B]}{[S]_0}t \tag{5.7}$$

The decay of the labile fraction of DOM was analysed essentially according to the binary reaction model (Eqs. 5.2-5.4). We note, however, that $[B]$ is not strictly constant but increases with time. Neglecting this, we find in our crude analysis that the rate constant, k_l, is approximately an order of magnitude higher in the case of the cold extract compared to the hot (Table 5.1). As mentioned above, considering the very high TOC concentration that is being decomposed in the hot extract, compared to the aqueous oxygen solubility, this can possibly be explained by an oxygen deficiency in the hot extract that lowers k_l. The second model (Eqs. 5.5-5.7), on the other hand, approximately predicts that $k_l \sim 1/[S]_0$, which is close to what is obtained (Table 5.1). To summarise, we cannot from the present data set clearly discriminate between the two kinetic models discussed above. We recall that for a Taylor expansion of an exponential function to leading order $e^{-kt} = 1 - kt$. Measuring decomposition rates varying both $[S]_0$ and $[B]$, under conditions where there is no oxygen deficiency, would possibly provide information that allows for a more rigorous test of different kinetic models.

5.3 Colloidal DOM

The colloidal DOM persists bacterial decomposition. No change was observed in the scattering patterns of combined SAXS and SLS data from the first and last time points of incubation, for neither the cold nor the hot extract, as shown in Figure 5.3.

The broad resonances remaining in the ^{1}H NMR spectra after the incubation period are assumed to originate from the colloidal material, and these resonances were similar in the two extracts (Figure 5.4). The resonances correspond to carbohydrates (R4) and likely aliphatic –CH_3 and –CH_2– groups (0.8 and 1.2 ppm). The origin of the small signal around 1.9–2.1 ppm is currently uncertain, but it could come from carbon double bonds in lipids[153].

We used our calibration curve described in Section 3.1.2 to quantify the NMR signal remaining after two months. To convert the proton signal to a carbon concentration, we assumed the full intensity to come from carbohydrates. Using the formula $(C_5O_4H_8)_n$, assuming two OH-groups which exchange with water as in the previous chapter, this gave a C/H ratio of 5/6. The resulting calculated carbon concentration was roughly half of the measured remaining TOC, for both the cold and the hot extract. It is still unclear how much of the signal from colloidal DOM we are able to resolve in the ^{1}H NMR spectra, and there are a number of possible reasons for the factor 2 difference in the quantification, which are more thoroughly discussed in the SI of Paper III. Primarily, we could have resonances extending far beyond the integrated area of 0.6–9 ppm due to slow motion, which would also give an uncertainty in the identification of the baseline. There is also an uncertainty in the C/H ratio used and we may lose some signal in the region excluded due to water suppression.

5.3.1 Revised structural model

From the results described above, we make an important observation regarding our interpretation of the colloidal structure of the smaller colloids. If these would be free polymer coils of carbohydrates as previously modelled, they would have fast internal motion and produce sharp resonances in the NMR spectra (compare for example with the spectrum of dissolved cellulose in Hagman et al.[154]). However, no such peaks were observed after incubation, while at the same time the scattering signal from this colloidal species remained unchanged (Figure 5.3). This means that also the smaller colloids giving rise to the feature around $q \approx 0.1$ Å^{-1} must experience slow dynamics. The similarity of the ^{1}H NMR spectra from the cold and hot extracts after decomposition (Figure 5.4) suggests that the two colloidal species have similar dynamics, suggesting they have a similar structure. This indicate that the smaller

species is rather fragments of the larger one, and that we need to revise our structural model. At present, we do not have a clear picture of the structure of the smaller colloids. For simplicity, we describe them as smaller fractal aggregates, similar to the larger colloidal clusters.

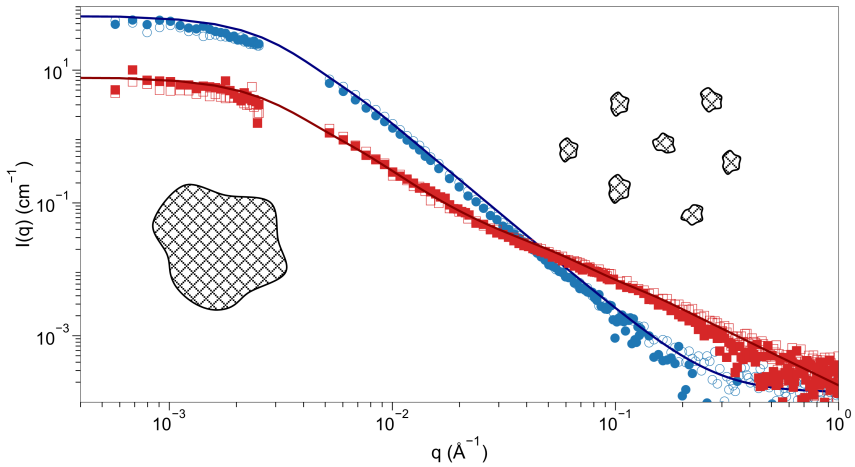

Figure 5.3 Combined SAXS and SLS data of cold (circles, blue) and hot (squares, red) DOM extracts from the first (open symbols) and last (filled symbols) time points of the incubation period. SLS samples were filtered 0.2 µm before measurements. Solid lines represent model calculations for a linear combination of fractal clusters based on Eq. 4.1, with parameters given in Table 5.2. Also shown are schematic illustrations of the large and small mass fractal clusters (not drawn to scale). Figure taken from Paper III.

Table 5.2 Parameters used for the model calculations of scattering data shown in Figure 5.3, for cold and hot extracts respectively. The TOC left after decomposition was 52 mg/l in the cold extract and 630 mg/l in the hot.

	Large cluster				Small cluster			
Extract	R_g	D	M	c	R_g	D	M	c
Cold[a]	60 nm	2.8	5×10^8 g/mol	110 mg/l	-	-	-	-
Hot[b]	60 nm	2.4	5×10^8 g/mol	13 mg/l	3 nm	1.6	1.5×10^4 g/mol	1400 mg/l

[a]If using data from a control sample at time 0 which was not filtered before SLS measurements, agreement was obtained using a large cluster with $R_g = 70$ nm and $M = 8 \times 10^8$ g/mol.
[b]If using data from a control sample at time 0 which was not filtered before SLS measurements, agreement was obtained using a large cluster with $R_g = 70$ nm and $M = 7 \times 10^8$ g/mol.

The scattering data could be modelled as previously described in Section 4.2.2, but using a second smaller mass fractal object instead of the coils for the hot extract (Figure 5.3). The scattering intensity of each species depends on the product of concentration and molar mass (Eq. 4.1). As the TOC remaining after the incubation is assumed

to be in colloidal form, the concentration used for the dominating colloidal species in the model calculation, was based on the TOC measured after 2 months (52 mg/l in the cold extract and 630 mg/l in the hot) multiplied by a factor of 2.2. The factor of 2.2 is the ration between the molecular weight of the monomeric unit and total atomic weight of carbon in that unit, for a material like hemicellulose. In the cold extracts, the large 200 nm clusters constitute the dominating colloidal species, while in the hot extracts, the smaller colloidal species dominate in concentration, based on the scattering data. With the model concentrations fixed from TOC, the molecular weights of the respective clusters were varied to obtain agreement with the scattering data. The model parameters are given in Table 5.2.

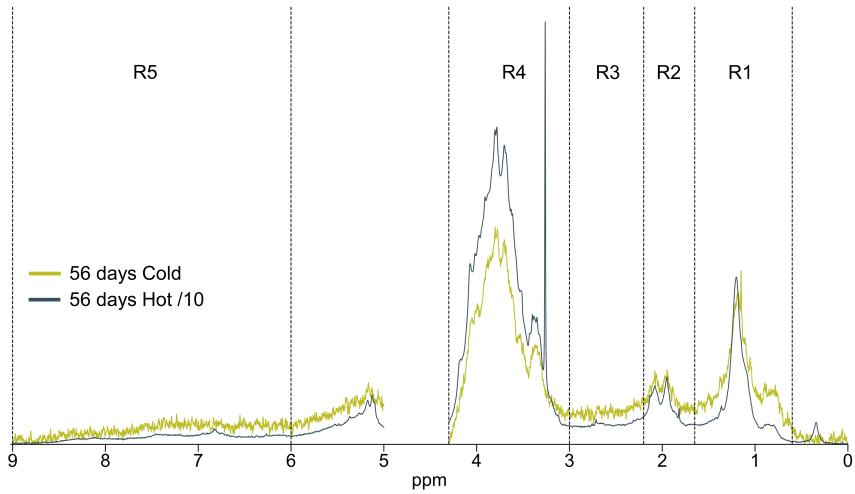

Figure 5.4 ^{1}H NMR spectra of the hot and cold extracts at day 56 of incubation. The spectra of the hot extract is divided by a factor of 10. The sharp resonance at 3.3 ppm in the hot extract is assumed to come from methanol. Dashed lines represent the regions of different compound classes described in Section 4.1.

5.4 Conclusions

The results of this chapter has provided us with an important piece of information to add to our puzzle. That is: the colloidal material constituted the stable fraction of our extracts. Our previous observation, that the colloidal fraction constitutes roughly half of the DOM (Section 4.2), meaning half of the TOC was non-colloidal, agrees nicely with the total fraction of TOC that was removed during incubation. At the same time, the scattering results suggest that colloids remained intact. This combined with the removal of all sharp peaks in NMR, and the similarity in decomposition kinetics for TOC and NMR intensity, leads us to the conclusion that molecular DOM is readily

decomposed by the bacteria, while colloidal DOM persists decomposition.

The decomposition experiment thus provided us with the opportunity to investigate the isolated colloidal fraction. From this we concluded that the smaller colloidal species found in hot extracts is likely not free polymer coils, as this structure would result in sharp peaks in the ^{1}H NMR spectra. We therefore revise our structural model and describe the colloids as two different size fractions of mass fractal clusters.

6 Interactions of Dissolved Organic Matter and Hematite nanoparticles

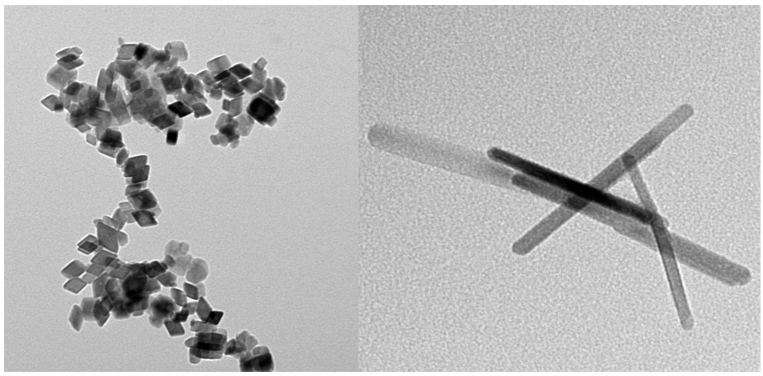

TEM micrographs of synthesised hematite and goethite particles.

In this chapter, we discuss the interactions between DOM and hematite particles, based on the findings presented in Paper IV. As DOM and minerals are in close proximity throughout terrestrial and aquatic systems, these interactions are important for the fate of both species. The formation of mineral-organic associations[48], with accompanying changes in size, charge and colloidal stability, could influence for example mobility, sedimentation rate and bioavailability. With our understanding of colloidal and molecular DOM, based on the puzzle pieces of Chapter 4, we here utilise cryo-TEM and the contrast variation possibilities of neutron scattering, to study mixtures of organic and inorganic components.

6.1 The hematite particles

Hematite nanoparticles were synthesised and the solvent exchanged to aqueous solutions having a pH=5.5, and a volume fraction of D_2O (ϕ_{D_2O}) of 1 or 0.3, as described in Section 2.3. These two compositions correspond to low (HEM_1) and high ($HEM_{0.3}$) neutron scattering contrast respectively, based on a neutron SLD of $\rho_n = 7.2 \times 10^{10} \text{cm}^{-2}$, calculated from the chemical formula Fe_2O_3 and a mass density of 5.26 g/cm^3 [100]. The synthesised hematite particles had an isoelectric point around pH 8.5 and showed a positive ζ-potential of ca. 25 mV at the pH used.

As described in Section 2.3, cryo-TEM showed that primary hematite particles were aggregated. The aggregates had a $\langle R_H \rangle$ of ca. 70 nm, meaning they are of a similar size as the colloidal DOM. The aggregates were stable over a wide range of dilutions and pH, and no further aggregation was observed with time. We hence conclude that the aggregation was effectively irreversible and a consequence of the synthesis protocol. The reason for this aggregation was not further investigated.

The SANS pattern of $HEM_{0.3}$ is shown in Figure 6.1. The data is compared with, and fairly well described by, a model calculation of particles forming mass fractal aggregates[155]. The model aggregates are described by a correlation length, $\xi = 45$ nm, a fractal dimension $D = 2.2$, and a radius $R = 10$ nm of the primary particle, which for simplicity is assumed to be spherical.

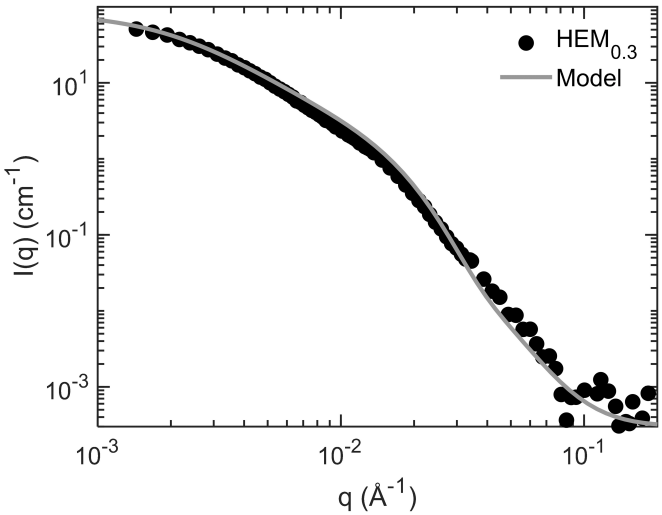

Figure 6.1 SANS pattern of hematite at ϕ_{D_2O} =0.3 and a concentration of 528 mg/l. The data is compared with a model calculation of mass fractal aggregates of spherical particles.

6.2 DOM-hematite mixtures

DOM was extracted at room temperature, also using solutions of ϕ_{D_2O} =1 or 0.3 respectively (DOM_1, $DOM_{0.3}$). As discussed in Section 4.2.4, the extracted DOM has a match point around 40% D_2O, meaning the different contrast conditions used allow us to highlight the scattering from hematite (at ϕ_{D_2O} =0.3) or DOM (at ϕ_{D_2O} =1) individually. The DOM extracts had a pH of 5.5 and both showed a ζ-potential of ca. -15 mV. As colloidal DOM and the hematite nanoparticles are oppositely charged, one may expect attractive interactions.

SANS patterns of $HEM_{0.3}$, mixed with $DOM_{0.3}$ at different concentrations, are shown in Figure 6.2 A. At high q, corresponding to the primary particle size, the scattering pattern is practically unaffected by the addition of DOM. At lower q-values on the other hand, there is an increase in intensity and the region of power law scattering is extended. This indicate that the hematite flocculated into structures larger than the resolution limit of the experiment. The scattering contribution from $DOM_{0.3}$, also shown in Figure 6.2 A, is negligible.

Cryo-TEM images of the mixtures confirmed the SANS data (Figure 6.2 B). Large hematite flocs (several µm) are observed, without any distinguishable DOM clusters incorporated. The ζ-potential of the mixtures was ca. -25 mV, and as the light scattering signal is dominated by the mineral particles (ca. five times higher scattering

intensity than DOM at equal concentrations), this suggests a charge reversal of the hematite in the flocculated state.

The structure of colloidal DOM was unaffected by the presence of the hematite particles. SANS data of DOM_1, mixed with different concentrations of HEM_1, is shown in Figure 6.2 C. The scattering pattern agrees with our previous model of colloidal DOM clusters, and no change is observed over the full q-range for any hematite concentration measured.

So what makes the hematite flocculate? As the colloidal DOM seems unaffected by the mineral particles, it is likely the low molecular weight fraction of DOM which adsorb and cause charge reversal and flocculation of the mineral. This could be due to faster diffusion and adsorption kinetics of smaller species. Once a net negative charge is obtained, negatively charged colloidal DOM is repelled from the flocs. Such a charge reversal can be caused by the binding of polyanions, leading to an overcompensation of the surface charge[156]. Polyanions may also cause bridging[1] between the original hematite aggregates, promoting the flocculation. Possibly, such polyanions in DOM could be oxidised carbohydrates. That mainly the low molecular weight fraction of DOM adsorb and promotes the flocculation of positively charged mineral particles has been proposed previously[157]. It would be interesting to perform similar studies using dialysed DOM, where the small molecules have been removed, to further test this idea.

In Chapter 5, we concluded that the low molecular weight fraction of DOM constituted the main part of the labile fraction. Here we observe mainly this fraction to adsorb onto mineral particles. If the adsorption provides a physical protection of DOM against microbial decomposition[48,53,55], the formation of such MOA may play an important role for the preservation of this DOM fraction. This remains to be further investigated in future studies.

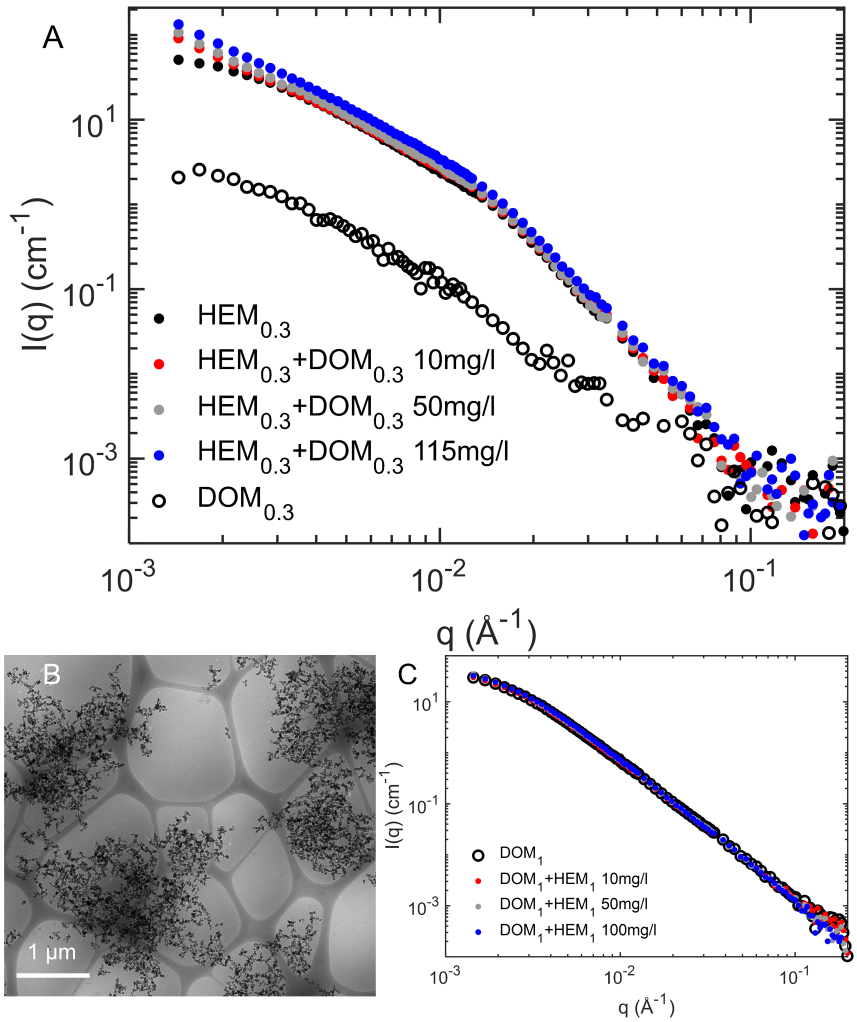

Figure 6.2 A) SANS patterns of hematite at a concentration of 528 mg/l, mixed with DOM at TOC concentrations of 10, 50 and 115 mg/l for $\phi_{D_2O} = 0.3$. Also shown is the scattering signal of DOM alone, at a TOC concentration of 115 mg/l. B) Cryo-TEM image of $HEM_{0.3}$ at a concentration of 528 mg/l mixed with $DOM_{0.3}$ at a TOC of 10 mg/l. The scale bar corresponds to 1 µm. C) SANS patterns of DOM at a TOC of 123 mg/l mixed with hematite to final concentrations of 10, 50 or 100 mg/l, for $\phi_{D_2O} = 1$. Figure taken from Paper IV.

Epilogue

With this thesis, we have made an attempt to solve the puzzle of DOM, and paint a picture of its characteristics from the molecular to colloidal length scale. I can not say that we have reached our final goal, but we have made progress. By means of our multi-method approach, we have established a model for DOM, based on which we have assessed bacterial decomposition and mineral interactions. We have shown that scattering techniques constitute a valuable tool in this kind of DOM studies. Our combined results demonstrate that colloidal properties needs to be considered when trying to predict the fate of DOM.

Several questions still remains to be addressed. We have concluded that the main chemical component of the investigated DOM extracts correspond to carbohydrates, based mainly on NMR characterisation. Are there chemical species which we have missed due to our choice of method? What would we find if using e.g. mass spectrometry? Also, in Chapter 5 we saw that our smaller colloidal species is likely not a random-walk polymer coil. The precise structure remains to be resolved and this could possibly be done using scattering techniques, if it is possible to isolate this species, or by using atomic force microscopy. If the "coils" and "clusters" could be isolated, it would also be possible to study their individual composition more closely. An alternative for this could be to use a spectroscopy technique with spatial resolution, e.g. electron energy loss spectroscopy in a cryo-TEM.

Further studies are needed to resolve the impact of different microbial species on the decomposition of colloidal DOM, e.g. a comparison between the effect of fungi and bacteria. It would also be interesting to see the effect of mineral particles on the DOM decomposition and how isolated colloidal DOM would interact with mineral particles.

The most important question however, is probably how our results relate to real processes taking place in different environmental systems. We have only studied DOM extracted from one type of soil using a pre-defined size cut-off. Would we find vastly

different colloidal species using different filter sizes? Are there large differences in the properties of colloids from different soils? Do our results apply also to DOM from aquatic systems? To resolve these kinds of questions would require extensive screening studies, likely involving the use of a synchrotron source.

As we continue changing the conditions for life on this planet, a thorough understanding of something as fundamental as the carbon cycle is needed. For those who think we already know what is needed about soil, I hope that after reading this thesis you agree with me when I say: we have only scratched the surface.

References

[1] Evans, D. F.; Wennerström, H. *The Colloidal Domain: Where Physics, Chemistry, Biology, and Technology Meet*, 2nd ed.; Advances in Interfacial Engineering Series; Wiley-VCH: New York, 1999.

[2] Myers, D. *Surfaces, Interfaces, and Colloids: Principles and Applications*, 2nd ed.; Wiley-VCH: New York, 1999.

[3] IUSS Working Group WRB, *World Reference Base for Soil Resources. International Soil Classification System for Naming Soils and Creating Legends for Soil Maps*, 4th ed.; International Union of Soil Sciences (IUSS): Vienna, Austria, 2022.

[4] Lal, R. Carbon Management in Agricultural Soils. *Mitig. Adapt. Strat. Glob. Change* **2007**, *12*, 303–322.

[5] Xu, X.; Pei, J.; Xu, Y.; Wang, J. Soil Organic Carbon Depletion in Global Mollisols Regions and Restoration by Management Practices: A Review. *J. Soils Sediments* **2020**, *20*, 1173–1181.

[6] Lal, R. Soil Carbon Sequestration Impacts on Global Climate Change and Food Security. *Science* **2004**, *304*, 1623–1627.

[7] Sokol, N. W.; Sanderman, J.; Bradford, M. A. Pathways of Mineral-associated Soil Organic Matter Formation: Integrating the Role of Plant Carbon Source, Chemistry, and Point of Entry. *Glob. Change Biol.* **2019**, *25*, 12–24.

[8] Cotrufo, M. F.; Soong, J. L.; Horton, A. J.; Campbell, E. E.; Haddix, M. L.; Wall, D. H.; Parton, W. J. Formation of Soil Organic Matter via Biochemical and Physical Pathways of Litter Mass Loss. *Nature Geosci.* **2015**, *8*, 776–779.

[9] Schmidt, M. W. I.; Torn, M. S.; Abiven, S.; Dittmar, T.; Guggenberger, G.; Janssens, I. A.; Kleber, M.; Kögel-Knabner, I.; Lehmann, J.; Manning, D. A. C.; Nannipieri, P.; Rasse, D. P.; Weiner, S.; Trumbore, S. E. Persistence of Soil Organic Matter as an Ecosystem Property. *Nature* **2011**, *478*, 49–56.

[10] Kleber, M.; Johnson, M. G. *Advances in Agronomy*; Elsevier, 2010; Vol. 106; pp 77–142.

[11] Lehmann, J.; Kleber, M. The Contentious Nature of Soil Organic Matter. *Nature* **2015**, *528*, 60–68.

[12] Trumbore, S. E. Potential Responses of Soil Organic Carbon to Global Environmental Change. *Proc. Natl. Acad. Sci. U.S.A.* **1997**, *94*, 8284–8291.

[13] Tranvik, L. J. et al. Lakes and Reservoirs as Regulators of Carbon Cycling and Climate. *Limnol. Oceanogr.* **2009**, *54*, 2298–2314.

[14] Dungait, J. A. J.; Hopkins, D. W.; Gregory, A. S.; Whitmore, A. P. Soil Organic Matter Turnover Is Governed by Accessibility Not Recalcitrance. *Glob. Change Biol.* **2012**, *18*, 1781–1796.

[15] Abramoff, R.; Xu, X.; Hartman, M.; O'Brien, S.; Feng, W.; Davidson, E.; Finzi, A.; Moorhead, D.; Schimel, J.; Torn, M.; Mayes, M. A. The Millennial Model: In Search of Measurable Pools and Transformations for Modeling Soil Carbon in the New Century. *Biogeochemistry* **2018**, *137*, 51–71.

[16] Huntzinger, D. N. et al. Uncertainty in the Response of Terrestrial Carbon Sink to Environmental Drivers Undermines Carbon-Climate Feedback Predictions. *Sci. Rep.* **2017**, *7*, 4765.

[17] Lehmann, J.; Kinyangi, J.; Solomon, D. Organic Matter Stabilization in Soil Microaggregates: Implications from Spatial Heterogeneity of Organic Carbon Contents and Carbon Forms. *Biogeochemistry* **2007**, *85*, 45–57.

[18] Haddaway, N. R.; Hedlund, K.; Jackson, L. E.; Kätterer, T.; Lugato, E.; Thomsen, I. K.; Jørgensen, H. B.; Isberg, P.-E. How Does Tillage Intensity Affect Soil Organic Carbon? A Systematic Review. *Environ. Evid.* **2017**, *6*, 30.

[19] Ledesma, J. L.; Köhler, S. J.; Futter, M. N. Long-Term Dynamics of Dissolved Organic Carbon: Implications for Drinking Water Supply. *Sci. Total Environ.* **2012**, *432*, 1–11.

[20] Kritzberg, E. S.; Hasselquist, E. M.; Škerlep, M.; Löfgren, S.; Olsson, O.; Stadmark, J.; Valinia, S.; Hansson, L.-A.; Laudon, H. Browning of Freshwaters: Consequences to Ecosystem Services, Underlying Drivers, and Potential Mitigation Measures. *Ambio* **2020**, *49*, 375–390.

[21] Kothawala, D. N.; Kellerman, A. M.; Catalán, N.; Tranvik, L. J. Organic Matter Degradation across Ecosystem Boundaries: The Need for a Unified Conceptualization. *Trends Ecol. Evol.* **2021**, *36*, 113–122.

[22] v. Lützow, M.; Kögel-Knabner, I.; Ekschmitt, K.; Matzner, E.; Guggenberger, G.; Marschner, B.; Flessa, H. Stabilization of Organic Matter in Temperate Soils: Mechanisms and Their Relevance under Different Soil Conditions - a Review: Mechanisms for Organic Matter Stabilization in Soils. *Eur. J. Soil Sci.* **2006**, *57*, 426–445.

[23] Berg, B.; Laskowski, R. *Advances in Ecological Research*; Elsevier, 2005; Vol. 38; pp 73–100.

[24] Weiss, M. S.; Abele, U.; Weckesser, J.; Welte, W.; Schiltz, E.; Schulz, G. E. Molecular Architecture and Electrostatic Properties of a Bacterial Porin. *Science* **1991**, *254*, 1627–1630.

[25] Hedges, J.; Oades, J. Comparative Organic Geochemistries of Soils and Marine Sediments. *Org. Geochem.* **1997**, *27*, 319–361.

[26] Nagata, T. In *Microbial Ecology of the Oceans*; Kirchman, D. L., Ed.; John Wiley & Sons, Inc.: Hoboken, NJ, USA, 2008; pp 207–241.

[27] Berggren, M.; Guillemette, F.; Bieroza, M.; Buffam, I.; Deininger, A.; Hawkes, J. A.; Kothawala, D. N.; LaBrie, R.; Lapierre, J.-F.; Murphy, K. R.; Al-Kharusi, E. S.; Rulli, M. P. D.; Hensgens, G.; Younes, H.; Wünsch, U. J. Unified Understanding of Intrinsic and Extrinsic Controls of Dissolved Organic Carbon Reactivity in Aquatic Ecosystems. *Ecology* **2022**, *103*.

[28] Bremner, J. M.; Lees, H. Studies on Soil Organic Matter: Part II. The Extraction of Organic Matter from Soil by Neutral Reagents. *J. Agric. Sci.* **1949**, *39*, 274–279.

[29] Herbert, B. E.; Bertsch, P. M. In *Carbon Forms and Functions in Forest Soils*; McFee, W. W., Kelly, J. M., Eds.; Soil Science Society of America: Madison, WI, USA, 1995; pp 63–88.

[30] Davidson, E. A.; Galloway, L. F.; Strand, M. K. Assessing Available Carbon: Comparison of Techniques across Selected Forest Soils. *Commun. Soil Sci. Plant Anal* **1987**, *18*, 45–64.

[31] Chen, X.; Jin, M.; Xu, Y.; Chu, W.; Olk, D. C.; Hu, J.; Jiang, Y.; Mao, J.; Gao, H.; Thompson, M. L. Potential Alterations in the Chemical Structure of Soil Organic Matter Components during Sodium Hydroxide Extraction. *J. Environ. Qual.* **2019**, *48*, 1578–1586.

[32] Achard, F. C. Chemische Untersuchung Des Torfs. *Crell's Chem. Ann.* **1786**, *2*, 391–403.

[33] Aiken, G. R., McKnight, D. M., Wershaw, R. L., MacCarthy, P., Eds. *Humic Substances in Soil, Sediment, and Water: Geochemistry, Isolation, and Characterization*; Wiley: New York, 1985.

[34] Olk, D. C.; Bloom, P. R.; De Nobili, M.; Chen, Y.; McKnight, D. M.; Wells, M. J. M.; Weber, J. Using Humic Fractions to Understand Natural Organic Matter Processes in Soil and Water: Selected Studies and Applications. *J. Environ. Qual.* **2019**, *48*, 1633–1643.

[35] Swift, R. S. In *SSSA Book Series*; Sparks, D., Page, A., Helmke, P., Loeppert, R., Soltanpour, P. N., Tabatabai, M. A., Johnston, C. T., Sumner, M. E., Eds.; Soil Science Society of America, American Society of Agronomy: Madison, WI, USA, 1996; pp 1011–1069.

[36] Thurman, E. M.; Malcolm, R. L. Preparative Isolation of Aquatic Humic Substances. *Environ. Sci. Technol.* **1981**, *15*, 463–466.

[37] Sutton, R.; Sposito, G. Molecular Structure in Soil Humic Substances: The New View. *Environ. Sci. Technol.* **2005**, *39*, 9009–9015.

[38] Simpson, A. J.; Song, G.; Smith, E.; Lam, B.; Novotny, E. H.; Hayes, M. H. B. Unraveling the Structural Components of Soil Humin by Use of Solution-State Nuclear Magnetic Resonance Spectroscopy. *Environ. Sci. Technol.* **2007**, *41*, 876–883.

[39] Kelleher, Brian. P.; Simpson, Andre. J. Humic Substances in Soils: Are They Really Chemically Distinct? *Environ. Sci. Technol.* **2006**, *40*, 4605–4611.

[40] Kalbitz, K.; Schmerwitz, J.; Schwesig, D.; Matzner, E. Biodegradation of Soil-Derived Dissolved Organic Matter as Related to Its Properties. *Geoderma* **2003**, *113*, 273–291.

[41] Uselman, S. M.; Qualls, R. G.; Lilienfein, J. Quality of Soluble Organic C, N, and P Produced by Different Types and Species of Litter: Root Litter versus Leaf Litter. *Soil Biol. Biochem.* **2012**, *54*, 57–67.

[42] Kiikkilä, O.; Kitunen, V.; Smolander, A. Dissolved Soil Organic Matter from Surface Organic Horizons under Birch and Conifers: Degradation in Relation to Chemical Characteristics. *Soil Biol. Biochem.* **2006**, *38*, 737–746.

[43] Chapin, F. S.; Matson, P. A.; Vitousek, P. M. *Principles of Terrestrial Ecosystem Ecology*; Springer New York: New York, NY, 2011; pp 183–228.

[44] Capriel, P. Hydrophobicity of Organic Matter in Arable Soils: Influence of Management. *Eur. J. Soil Sci.* **1997**, *48*, 457–462.

[45] Marschner, B.; Kalbitz, K. Controls of Bioavailability and Biodegradability of Dissolved Organic Matter in Soils. *Geoderma* **2003**, *113*, 211–235.

[46] Shen, Y.; Benner, R. Molecular Properties Are a Primary Control on the Microbial Utilization of Dissolved Organic Matter in the Ocean. *Limnol. Oceanogr.* **2020**, *65*, 1061–1071.

[47] Kleber, M.; Nico, P. S.; Plante, A.; Filley, T.; Kramer, M.; Swanston, C.; Sollins, P. Old and Stable Soil Organic Matter Is Not Necessarily Chemically Recalcitrant: Implications for Modeling Concepts and Temperature Sensitivity: SLOW TURNOVER OF LABILE SOIL ORGANIC MATTER. *Glob. Change Biol.* **2011**, *17*, 1097–1107.

[48] Kleber, M.; Eusterhues, K.; Keiluweit, M.; Mikutta, C.; Mikutta, R.; Nico, P. S. *Advances in Agronomy*; Elsevier, 2015; Vol. 130; pp 1–140.

[49] Bastviken, D.; Persson, L.; Odham, G.; Tranvik, L. Degradation of Dissolved Organic Matter in Oxic and Anoxic Lake Water. *Limnol. Oceanogr.* **2004**, *49*, 109–116.

[50] Rousk, J.; Jones, D. L. Loss of Low Molecular Weight Dissolved Organic Carbon (DOC) and Nitrogen (DON) in H2O and 0.5M K2SO4 Soil Extracts. *Soil Biol. Biochem.* **2010**, *42*, 2331–2335.

[51] Pietikäinen, J.; Pettersson, M.; Bååth, E. Comparison of Temperature Effects on Soil Respiration and Bacterial and Fungal Growth Rates. *FEMS Microbiol. Ecol.* **2005**, *52*, 49–58.

[52] Boyer, J.; Groffman, P. Bioavailability of Water Extractable Organic Carbon Fractions in Forest and Agricultural Soil Profiles. *Soil Biol. Biochem.* **1996**, *28*, 783–790.

[53] Kalbitz, K.; Schwesig, D.; Rethemeyer, J.; Matzner, E. Stabilization of Dissolved Organic Matter by Sorption to the Mineral Soil. *Soil Biol. Biochem.* **2005**, *37*, 1319–1331.

[54] Tang, N.; Siebers, N.; Leinweber, P.; Eckhardt, K.-U.; Dultz, S.; Nischwitz, V.; Klumpp, E. Implications of Free and Occluded Fine Colloids for Organic Matter Preservation in Arable Soils. *Environ. Sci. Technol.* **2022**, acs.est.2c01973.

[55] Kögel-Knabner, I.; Guggenberger, G.; Kleber, M.; Kandeler, E.; Kalbitz, K.; Scheu, S.; Eusterhues, K.; Leinweber, P. Organo-mineral Associations in Temperate Soils: Integrating Biology, Mineralogy, and Organic Matter Chemistry. *J. Plant Nutr. Soil Sci.* **2008**, *171*, 61–82.

[56] Chevallier, T.; Muchaonyerwa, P.; Chenu, C. Microbial Utilisation of Two Proteins Adsorbed to a Vertisol Clay Fraction: Toxin from Bacillus Thuringiensis Subsp. Tenebrionis and Bovine Serum Albumin. *Soil Biol. Biochem.* **2003**, *35*, 1211–1218.

[57] Lammirato, C.; Miltner, A.; Wick, L. Y.; Kästner, M. Hydrolysis of Cellobiose by β-Glucosidase in the Presence of Soil Minerals – Interactions at Solid–Liquid Interfaces and Effects on Enzyme Activity Levels. *Soil Biol. Biochem.* **2010**, *42*, 2203–2210.

[58] Kaiser, K.; Kalbitz, K. Cycling Downwards – Dissolved Organic Matter in Soils. *Soil Biol. Biochem.* **2012**, *52*, 29–32.

[59] Zimmerman, A. R.; Ahn, M.-Y. In *Soil Enzymology*; Shukla, G., Varma, A., Eds.; Springer Berlin Heidelberg: Berlin, Heidelberg, 2010; Vol. 22; pp 271–292.

[60] Wang, T.; Tian, Z.; Tunlid, A.; Persson, P. Nitrogen Acquisition from Mineral-associated Proteins by an Ectomycorrhizal Fungus. *New Phytol.* **2020**, *228*, 697–711.

[61] Lalonde, K.; Mucci, A.; Ouellet, A.; Gélinas, Y. Preservation of Organic Matter in Sediments Promoted by Iron. *Nature* **2012**, *483*, 198–200.

[62] Hemingway, J. D.; Rothman, D. H.; Grant, K. E.; Rosengard, S. Z.; Eglinton, T. I.; Derry, L. A.; Galy, V. V. Mineral Protection Regulates Long-Term Global Preservation of Natural Organic Carbon. *Nature* **2019**, *570*, 228–231.

[63] Kritzberg, E. S.; Bedmar Villanueva, A.; Jung, M.; Reader, H. E. Importance of Boreal Rivers in Providing Iron to Marine Waters. *PLoS ONE* **2014**, *9*, e107500.

[64] Herzog, S. D.; Gentile, L.; Olsson, U.; Persson, P.; Kritzberg, E. S. Characterization of Iron and Organic Carbon Colloids in Boreal Rivers and Their Fate at High Salinity. *J. Geophys. Res. Biogeosci.* **2020**, *125*.

[65] Kaiser, K.; Guggenberger, G. The Role of DOM Sorption to Mineral Surfaces in the Preservation of Organic Matter in Soils. *Org. Geochem.* **2000**, *31*, 711–725.

[66] Hur, J.; Schlautman, M. A. Molecular Weight Fractionation of Humic Substances by Adsorption onto Minerals. *J. Colloid Interface Sci.* **2003**, *264*, 313–321.

[67] Kaiser, K.; Zech, W. Competitive Sorption of Dissolved Organic Matter Fractions to Soils and Related Mineral Phases. *Soil Sci. Soc. Am. J.* **1997**, *61*, 64–69.

[68] Gu, B.; Mehlhorn, T. L.; Liang, L.; McCarthy, J. F. Competitive Adsorption, Displacement, and Transport of Organic Matter on Iron Oxide: I. Competitive Adsorption. *Geochim. Cosmochim. Acta* **1996**, *60*, 1943–1950.

[69] Lv, J.; Zhang, S.; Wang, S.; Luo, L.; Cao, D.; Christie, P. Molecular-Scale Investigation with ESI-FT-ICR-MS on Fractionation of Dissolved Organic Matter Induced by Adsorption on Iron Oxyhydroxides. *Environ. Sci. Technol.* **2016**, *50*, 2328–2336.

[70] Curti, L.; Moore, O. W.; Babakhani, P.; Xiao, K.-Q.; Woulds, C.; Bray, A. W.; Fisher, B. J.; Kazemian, M.; Kaulich, B.; Peacock, C. L. Carboxyl-Richness Controls Organic Carbon Preservation during Coprecipitation with Iron (Oxyhydr)Oxides in the Natural Environment. *Commun. Earth. Environ.* **2021**, *2*, 229.

[71] Six, J.; Bossuyt, H.; Degryze, S.; Denef, K. A History of Research on the Link between (Micro)Aggregates, Soil Biota, and Soil Organic Matter Dynamics. *Soil Tillage Res.* **2004**, *79*, 7–31.

[72] Mueller, C. W.; Schlund, S.; Prietzel, J.; Kögel-Knabner, I.; Gutsch, M. Soil Aggregate Destruction by Ultrasonication Increases Soil Organic Matter Mineralization and Mobility. *Soil Sci. Soc. Am. J.* **2012**, *76*, 1634–1643.

[73] Goebel, M.-O.; Bachmann, J.; Woche, S. K.; Fischer, W. R. Soil Wettability, Aggregate Stability, and the Decomposition of Soil Organic Matter. *Geoderma* **2005**, *128*, 80–93.

[74] Tisdall, J. M.; Oades, J. M. Organic Matter and Water-Stable Aggregates in Soils. *J. Soil Sci.* **1982**, *33*, 141–163.

[75] Totsche, K. U.; Amelung, W.; Gerzabek, M. H.; Guggenberger, G.; Klumpp, E.; Knief, C.; Lehndorff, E.; Mikutta, R.; Peth, S.; Prechtel, A.; Ray, N.; Kögel-Knabner, I. Microaggregates in Soils. *J. Plant Nutr. Soil Sci.* **2018**, *181*, 104–136.

[76] Churchman, G. J. The Philosophical Status of Soil Science. *Geoderma* **2010**, *157*, 214–221.

[77] Six, J.; Conant, R. T.; Paul, E. A.; Paustian, K. Stabilization Mechanisms of Soil Organic Matter: Implications for C-saturation of Soils. *Plant Soil* **2002**, *241*, 155–176.

[78] Killham, K.; Amato, M.; Ladd, J. Effect of Substrate Location in Soil and Soil Pore-Water Regime on Carbon Turnover. *Soil Biol. Biochem.* **1993**, *25*, 57–62.

[79] Kellerman, A. M.; Kothawala, D. N.; Dittmar, T.; Tranvik, L. J. Persistence of Dissolved Organic Matter in Lakes Related to Its Molecular Characteristics. *Nature Geosci.* **2015**, *8*, 454–457.

[80] Lechtenfeld, O. J.; Kattner, G.; Flerus, R.; McCallister, S. L.; Schmitt-Kopplin, P.; Koch, B. P. Molecular Transformation and Degradation of Refractory Dissolved Organic Matter in the Atlantic and Southern Ocean. *Geochim. Cosmochim. Acta* **2014**, *126*, 321–337.

[81] Mosher, J. J.; Kaplan, L. A.; Podgorski, D. C.; McKenna, A. M.; Marshall, A. G. Longitudinal Shifts in Dissolved Organic Matter Chemogeography and Chemodiversity within Headwater Streams: A River Continuum Reprise. *Biogeochemistry* **2015**, *124*, 371–385.

[82] Bolan, N. S.; Adriano, D. C.; Kunhikrishnan, A.; James, T.; McDowell, R.; Senesi, N. *Advances in Agronomy*; Elsevier, 2011; Vol. 110; pp 1–75.

[83] Yan, J.; Manelski, R.; Vasilas, B.; Jin, Y. Mobile Colloidal Organic Carbon: An Underestimated Carbon Pool in Global Carbon Cycles? *Front. Environ. Sci.* **2018**, *6*, 148.

[84] Jansen, B.; Kalbitz, K.; McDowell, W. H. Dissolved Organic Matter: Linking Soils and Aquatic Systems. *Vadose Zone J.* **2014**, *13*, vzj2014.05.0051.

[85] Kalbitz, K.; Angers, D.; Kaiser, K.; Chantigny, M. In *Soil Sampling and Methods of Analysis, Second Edition*; Carter, M., Gregorich, E., Eds.; CRC Press, 2007.

[86] Zsolnay, A. *Humic Substances in Terrestrial Ecosystems*; Elsevier, 1996; pp 171–223.

[87] Søndergaard, M.; Middelboe, M. A Cross-System Analysis of Labile Dissolved Organic Carbon. *Mar. Ecol. Prog. Ser.* **1995**, *118*, 283–294.

[88] Catalá, T. S.; Shorte, S.; Dittmar, T. Marine Dissolved Organic Matter: A Vast and Unexplored Molecular Space. *Appl. Microbiol. Biotechnol.* **2021**, *105*, 7225–7239.

[89] Findlay, S. E.; Parr, T. B. *Methods in Stream Ecology*; Elsevier, 2017; pp 21–36.

[90] Zsolnay, Á. Dissolved Organic Matter: Artefacts, Definitions, and Functions. *Geoderma* **2003**, *113*, 187–209.

[91] Lehmann, K.; Lehmann, R.; Totsche, K. U. Event-Driven Dynamics of the Total Mobile Inventory in Undisturbed Soil Account for Significant Fluxes of Particulate Organic Carbon. *Sci. Total Environ.* **2021**, *756*, 143774.

[92] Škerlep, M.; Nehzati, S.; Johansson, U.; Kleja, D. B.; Persson, P.; Kritzberg, E. S. Spruce Forest Afforestation Leading to Increased Fe Mobilization from Soils. *Biogeochemistry* **2022**, *157*, 273–290.

[93] Landgraf, D.; Leinweber, P.; Makeschin, F. Cold and Hot Water–Extractable Organic Matter as Indicators of Litter Decomposition in Forest Soils. *J. Plant Nutr. Soil Sci.* **2006**, *169*, 76–82.

[94] Chantigny, M. H.; Harrison-Kirk, T.; Curtin, D.; Beare, M. Temperature and Duration of Extraction Affect the Biochemical Composition of Soil Water-Extractable Organic Matter. *Soil Biol. Biochem.* **2014**, *75*, 161–166.

[95] Curtin, D.; Beare, M. H.; Chantigny, M. H.; Greenfield, L. G. Controls on the Extractability of Soil Organic Matter in Water over the 20 to 80°C Temperature Range. *Soil Sci. Soc. Am. J.* **2011**, *75*, 1423–1430.

[96] Guigue, J.; Mathieu, O.; Lévêque, J.; Mounier, S.; Laffont, R.; Maron, P. A.; Navarro, N.; Chateau, C.; Amiotte-Suchet, P.; Lucas, Y. A Comparison of Extraction Procedures for Water-Extractable Organic Matter in Soils. *Eur. J. Soil Sci.* **2014**, *65*, 520–530.

[97] Nkhili, E.; Guyot, G.; Vassal, N.; Richard, C. Extractability of Water-Soluble Soil Organic Matter as Monitored by Spectroscopic and Chromatographic Analyses. *Environ. Sci. Pollut. Res. Int.* **2012**, *19*, 2400–2407.

[98] Tönnersjöhedens försökspark. https://www.slu.se/institutioner/skoglig-faltforskning/forsoksparker/tonnersjohedens-forsokspark/tonnersjohedens-forsokspark/, Accessed 2022-12-30.

[99] Weil, R. R.; Brady, N. C. *The Nature and Properties of Soils*, fifteenth edition, global edition ed.; Pearson: Harlow, England London New York Boston San Francisco, 2017.

[100] Schwertmann, U.; Cornell, R. M. *Iron Oxides in the Laboratory: Preparation and Characterization*, 2nd ed.; Wiley-VCH: Weinheim ; New York, 2000.

[101] Hematite R110013 - RRUFF Database: Raman, X-ray, Infrared, and Chemistry. https://rruff.info/hematite/display=default/R110013, Accessed 2023-03-20.

[102] Demangeat, E.; Pédrot, M.; Dia, A.; Bouhnik-le-Coz, M.; Grasset, F.; Hanna, K.; Kamagate, M.; Cabello-Hurtado, F. Colloidal and Chemical Stabilities of Iron Oxide Nanoparticles in Aqueous Solutions: The Interplay of Structural, Chemical and Environmental Drivers. *Environ. Sci.: Nano* **2018**, *5*, 992–1001.

[103] Rodriguez, R. D.; Demaille, D.; Lacaze, E.; Jupille, J.; Chaneac, C.; Jolivet, J.-P. Rhombohedral Shape of Hematite Nanocrystals Synthesized via Thermolysis of an Additive-free Ferric Chloride Solution. *J. Phys. Chem. C* **2007**, *111*, 16866–16870.

[104] Hoover, C. M.; Hoover, C. M. *Field Measurements for Forest Carbon Monitoring: A Landscape-Scale Approach*; Springer Netherlands Springer e-books: Dordrecht, 2008.

[105] Cheremisinoff, N. P. *Polymer Characterization*; Elsevier, 1996; pp 43–81.

[106] Aceto, M.; Abollino, O.; Bruzzoniti, M. C.; Mentasti, E.; Sarzanini, C.; Malandrino, M. Determination of Metals in Wine with Atomic Spectroscopy (Flame-AAS, GF-AAS and ICP-AES); a Review. *Food Addit. Contam.* **2002**, *19*, 126–133.

[107] Keeler, J. *Understanding NMR Spectroscopy*, 2nd ed.; John Wiley and Sons: Chichester, U.K, 2010.

[108] Canet, D. *Nuclear Magnetic Resonance: Concepts and Methods*; Wiley: Chichester ; New York, 1996.

[109] Hwang, T.; Shaka, A. Water Suppression That Works. Excitation Sculpting Using Arbitrary Wave-Forms and Pulsed-Field Gradients. *J. Magn. Reson. A* **1995**, *112*, 275–279.

[110] Pines, A.; Gibby, M. G.; Waugh, J. S. Proton-Enhanced Nuclear Induction Spectroscopy. A Method for High Resolution NMR of Dilute Spins in Solids. *J. Chem. Phys.* **1972**, *56*, 1776–1777.

[111] Lindner, P., Zemb, T., Eds. *Neutrons, X-rays, and Light: Scattering Methods Applied to Soft Condensed Matter*, 1st ed.; North-Holland Delta Series; Elsevier: Amsterdam ; Boston, 2002.

[112] Glatter, O. *Scattering Methods and Their Application in Colloid and Interface Science*; Elsevier, 2018.

[113] Schurtenberger, P.; Newman, M. E. *Environmental Particles*, 1st ed.; CRC Press, 1993; pp 37–115.

[114] Pynn, R. Neutron Scattering – A Primer. *Los Alamos Science* **1990**,

[115] Lopez-Rubio, A.; Gilbert, E. P. Neutron Scattering: A Natural Tool for Food Science and Technology Research. *Trends Food Sci. Technol.* **2009**, *20*, 576–586.

[116] Martin-Bertelsen, B.; Andersson, E.; Köhnke, T.; Hedlund, A.; Stigsson, L.; Olsson, U. Revisiting the Dissolution of Cellulose in NaOH as "Seen" by X-rays. *Polymers* **2020**, *12*, 342.

[117] Siegert, A. J. F. *On the Fluctuations in Signals Returned by Many Independently Moving Scatterers*; 1943.

[118] Colliex, C. Seeing and Measuring with Electrons: Transmission Electron Microscopy Today and Tomorrow – An Introduction. *Comptes Rendus Physique* **2014**, *15*, 101–109.

[119] Danino, D. Cryo-TEM of Soft Molecular Assemblies. *Curr. Opin. Colloid Interface Sci.* **2012**, *17*, 316–329.

[120] Murata, K.; Wolf, M. Cryo-Electron Microscopy for Structural Analysis of Dynamic Biological Macromolecules. *Biochim. Biophys. Acta - Gen. Subj.* **2018**, *1862*, 324–334.

[121] Hunter, R. J. *Zeta Potential in Colloid Science: Principles and Applications*, 3rd ed.; Colloid Science 2; Academic Pr: London, 1988.

[122] Whitty, S. D.; Waggoner, D. C.; Cory, R. M.; Kaplan, L. A.; Hatcher, P. G. Direct Noninvasive 1 H NMR Analysis of Stream Water DOM: Insights into the Effects of Lyophilization Compared with Whole Water. *Magn. Reson. Chem.* **2019**,

[123] Field, L. D.; Hazari, N.; Li, H. L. Nitrogen Fixation Revisited on Iron(0) Dinitrogen Phosphine Complexes. *Inorg. Chem.* **2015**, *54*, 4768–4776.

[124] Wilson, M. A. APPLICATIONS OF NUCLEAR MAGNETIC RESONANCE SPECTROSCOPY TO THE STUDY OF THE STRUCTURE OF SOIL ORGANIC MATTER. *J. Soil Sci.* **1981**, *32*, 167–186.

[125] Hobbie, J. E.; Hobbie, E. A. Microbes in Nature Are Limited by Carbon and Energy: The Starving-Survival Lifestyle in Soil and Consequences for Estimating Microbial Rates. *Front. Microbiol.* **2013**, *4*.

[126] Soong, J. L.; Fuchslueger, L.; Marañon-Jimenez, S.; Torn, M. S.; Janssens, I. A.; Penuelas, J.; Richter, A. Microbial Carbon Limitation: The Need for Integrating Microorganisms into Our Understanding of Ecosystem Carbon Cycling. *Glob. Change Biol.* **2020**, *26*, 1953–1961.

[127] Gunina, A.; Kuzyakov, Y. Sugars in Soil and Sweets for Microorganisms: Review of Origin, Content, Composition and Fate. *Soil Biol. Biochem.* **2015**, *90*, 87–100.

[128] Ebringerová, A.; Hromádková, Z.; Heinze, T. In *Polysaccharides I*; Heinze, T., Ed.; Springer-Verlag: Berlin/Heidelberg, 2005; Vol. 186; pp 1–67.

[129] Lundqvist, J.; Teleman, A.; Junel, L.; Zacchi, G.; Dahlman, O.; Tjerneld, F.; Stålbrand, H. Isolation and Characterization of Galactoglucomannan from Spruce (Picea Abies). *Carbohydrate Polymers* **2002**, *48*, 29–39.

[130] Scheller, H. V.; Ulvskov, P. Hemicelluloses. *Annu. Rev. Plant Biol.* **2010**, *61*, 263–289.

[131] Günthardt-Goerg, M. S.; Keller, T.; Matyssek, R.; Scheidegger, C. Environmental Effects on Norway Spruce Needle Wax. *Forest Pathol.* **1994**, *24*, 92–111.

[132] Nikolić, B.; Todosijević, M.; Dordević, I.; Stanković, J.; Mitić, Z. S.; Tešević, V.; Marin, P. D. Nonacosan-10-Ol and *n* -Alkanes in Needles of *Pinus Halepensis*. *Nat. Prod. Commun.* **2020**, *15*, 1934578X2092097.

[133] Jarvie, H. P.; King, S. M. Small-Angle Neutron Scattering Study of Natural Aquatic Nanocolloids. *Environ. Sci. Technol.* **2007**, *41*, 2868–2873.

[134] Beaucage, G. Small-Angle Scattering from Polymeric Mass Fractals of Arbitrary Mass-Fractal Dimension. *J. Appl. Crystallogr.* **1996**, *29*, 134–146.

[135] Hammouda, B. Analysis of the Beaucage Model. *J. Appl. Crystallogr.* **2010**, *43*, 1474–1478.

[136] Pedersen, J. S.; Schurtenberger, P. Scattering Functions of Semiflexible Polymers with and without Excluded Volume Effects. *Macromolecules* **1996**, *29*, 7602–7612.

[137] Chen, W.-R.; Butler, P. D.; Magid, L. J. Incorporating Intermicellar Interactions in the Fitting of SANS Data from Cationic Wormlike Micelles. *Langmuir* **2006**, *22*, 6539–6548.

[138] Gatenholm, P., Tenkanen, M., Society, A. C., Society, A. C., Eds. *Hemicelluloses: Science and Technology*; ACS Symposium Series 864; American Chemical Society: Washington, DC, 2004.

[139] Ehrnrooth, E. M. L. Change in Pulp Fibre Density With Acid-Chlorite Delignification. *J. Wood Chem. Technol.* **1984**, *4*, 91–109.

[140] Gubitosi, M.; Duarte, H.; Gentile, L.; Olsson, U.; Medronho, B. On Cellulose Dissolution and Aggregation in Aqueous Tetrabutylammonium Hydroxide. *Biomacromolecules* **2016**, *17*, 2873–2881.

[141] Matas, A. Studies on the Structure of the Plant Wax Nonacosan-10-Ol, the Main Component of Epicuticular Wax Conifers. *Int. J. Biol. Macromol.* **2003**, *33*, 31–35.

[142] Bagger-Jörgensen, H.; Olsson, U.; Mortensen, K. Microstructure in a Ternary Microemulsion Studied by Small Angle Neutron Scattering. *Langmuir* **1997**, *13*, 1413–1421.

[143] Rissanen, J. V.; Murzin, D. Y.; Salmi, T.; Grénman, H. Aqueous Extraction of Hemicelluloses from Spruce – From Hot to Warm. *Bioresource Technology* **2016**, *199*, 279–282.

[144] Kishani, S.; Vilaplana, F.; Xu, W.; Xu, C.; Wågberg, L. Solubility of Softwood Hemicelluloses. *Biomacromolecules* **2018**, *19*, 1245–1255.

[145] Budtova, T.; Navard, P. Cellulose in NaOH–Water Based Solvents: A Review. *Cellulose* **2016**, *23*, 5–55.

[146] Gubitosi, M.; Nosrati, P.; Koder Hamid, M.; Kuczera, S.; Behrens, M. A.; Johansson, E. G.; Olsson, U. Stable, Metastable and Unstable Cellulose Solutions. *R. Soc. open sci.* **2017**, *4*, 170487.

[147] Melro, E.; Filipe, A.; Sousa, D.; Valente, A. J.; Romano, A.; Antunes, F. E.; Medronho, B. Dissolution of Kraft Lignin in Alkaline Solutions. *Int. J. Biol. Macromol.* **2020**, *148*, 688–695.

[148] Segad, M.; Hanski, S.; Olsson, U.; Ruokolainen, J.; Åkesson, T.; Jönsson, B. Microstructural and Swelling Properties of Ca and Na Montmorillonite: (In Situ) Observations with Cryo-TEM and SAXS. *J. Phys. Chem. C* **2012**, *116*, 7596–7601.

[149] Portillo, M. C.; Leff, J. W.; Lauber, C. L.; Fierer, N. Cell Size Distributions of Soil Bacterial and Archaeal Taxa. *Appl. Environ. Microbiol.* **2013**, *79*, 7610–7617.

[150] Westrich, J. T.; Berner, R. A. The Role of Sedimentary Organic Matter in Bacterial Sulfate Reduction: The *G* Model Tested1: Organics and Sulfate Reduction. *Limnol. Oceanogr.* **1984**, *29*, 236–249.

[151] Bowen, S. R.; Gregorich, E. G.; Hopkins, D. W. Biochemical Properties and Biodegradation of Dissolved Organic Matter from Soils. *Biol. Fertil. Soils.* **2009**, *45*, 733–742.

[152] Koehler, B.; von Wachenfeldt, E.; Kothawala, D.; Tranvik, L. J. Reactivity Continuum of Dissolved Organic Carbon Decomposition in Lake Water: REACTIVITY CONTINUUM OF LAKE DOC. *J. Geophys. Res. Biogeosci.* **2012**, *117*.

[153] Alexandri, E.; Ahmed, R.; Siddiqui, H.; Choudhary, M.; Tsiafoulis, C.; Gerothanassis, I. High Resolution NMR Spectroscopy as a Structural and Analytical Tool for Unsaturated Lipids in Solution. *Molecules* **2017**, *22*, 1663.

[154] Hagman, J.; Gentile, L.; Jessen, C. M.; Behrens, M.; Bergqvist, K.-E.; Olsson, U. On the Dissolution State of Cellulose in Cold Alkali Solutions. *Cellulose* **2017**, *24*, 2003–2015.

[155] Teixeira, J. Small-Angle Scattering by Fractal Systems. *J. Appl. Crystallogr.* **1988**, *21*, 781–785.

[156] Forsman, J. Surface Forces in Electrolytes Containing Polyions and Oppositely Charged Surfaces. *Curr. Opin. Colloid Interface Sci.* **2017**, *27*, 57–62.

[157] Gentile, L.; Wang, T.; Tunlid, A.; Olsson, U.; Persson, P. Ferrihydrite Nanoparticle Aggregation Induced by Dissolved Organic Matter. *J. Phys. Chem. A* **2018**, *122*, 7730–7738.

Scientific Publications

"...the mind is vaster, and the world ever so much more alive,
than I knew when I began."
– Michael Pollan

Printed by Media-Tryck, Lund 2023 NORDIC SWAN ECOLABEL 3041 0903

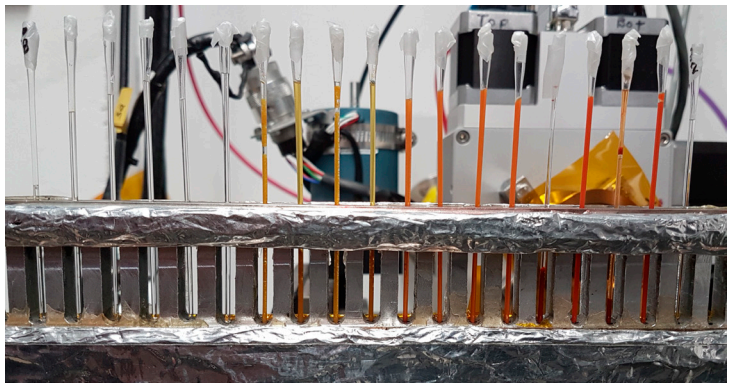

DISSOLVED ORGANIC MATTER (DOM) is an important component in the carbon cycle. To understand the mechanisms and kinetics controlling carbon storage, we must therefore also understand DOM. This thesis describes my work to characterise DOM from the molecular to colloidal length scale, using a combination of spectroscopy and scattering techniques. With this research, we try to combine the views of ecology and physical chemistry, to understand the role of colloidal size and structure in environmental processes.

LUND UNIVERSITY

ISBN 978-91-7422-956-1

Physical Chemistry
Faculty of Science
Lund University